Journal of Inflammation Research

Dovepress
Taylor & Francis Group

Open Access Full Text Article

ORIGINAL RESEARCH

Urolithin-C Suppresses Inflammation by Blocking NF-κB Signaling Pathway in LPS-Induced RAW 264.7 Macrophages

Vani Karadi Manjappa[1,2,*], Manjula Mavathuru Venkatappa[3,*], Deepadarshan Urs[4], Suliphuldevara Mathada Basavarajaiah[5], Shivakumar Venkataramaiah[3], Sanjana Bai Shivramsingh Mahendranathsingh[1], Sushma Mohan[1], Hunase Rajaiah Pushpavathi[4], Dharmappa Kattepura Krishnappa[4,*], Devaraja Sannaningaiah[1,*]

[1]Department of Studies and Research in Biochemistry, Tumkur University, Tumkur, Karnataka, 572103, India; [2]Department of Biochemistry, Maharani Lakshmi Ammanni College for Women, Autonomous, Bangalore, Karnataka, 560012, India; [3]Department of Studies and Research in Food Science and Nutrition, Tumkur University, Tumkur, Karnataka, 572103, India; [4]Inflammation Research Laboratory, Department of Studies and Research in Biochemistry, Mangalore University, Jnana Kaveri Postgraduate Centre, Kodagu, 571232, India; [5]P.G. Department of Chemistry, Vijaya College, Bangalore, 560004, India

*These authors contributed equally to this work

Correspondence: Devaraja Sannaningaiah, DOSR in Biochemistry, Tumkur University, Tumkur, Karnataka, 572103, India, Email sdevbiochem@gmail.com; Dharmappa Kattepura Krishnappa, Department of Biochemistry, Mangalore University, Karnataka, India, Email dharmappa@gmail.com

Purpose: In the current study, the evaluation of anti-inflammatory *(in vitro)* activity of chemically synthesized Urolithin-C was examined.

Methods: The synthesis of Urolithin-C (3,8,9-trihydroxy-6H-benzo[c]chromen-6-one) was carried out by chemical method and it was characterized using various techniques. The anti-inflammatory efficacy of synthesized Urolithin-C was studied by membrane stabilization, protein denaturation and protease inhibition assays. In addition, MTT (3-[4,5-dimethylthiazol-2-yl] 2,5-diphenyl tetrazolium bromide) assay was employed to evaluate the cytotoxic effect of Urolithin-C. The anti-inflammatory property of Urolithin-C was further examined using LPS (Lipopolysaccharide) induced RAW 264.7 (Mouse macrophage) cells. Furthermore, the anti-inflammatory properties of Urolithin-C was studied by quantifying pro/anti-inflammatory cytokines using ELISA (enzyme-linked immunosorbent assay). The mechanism of action of Urolithin-C on NF-κB (Nuclear Factor-kappa B) translocation was studied using CLSM (confocal laser scanning microscopy). While gene expression pattern was analyzed using RT-qPCR (Reverse Transcription quantitative Polymerase Chain Reaction).

Results: In comparison to the positive control aspirin, Urolithin-C showed a strong anti-inflammatory effect by preventing lysosomal degradation, protein denaturation and inhibition of protease. Furthermore, at the higher dose (200 µg/mL), Urolithin-C was found to be toxic to the mouse macrophages; however, at lower concentration (25 µg/mL) it did not cause toxicity to the said. Thus, 25 µg/mL of Urolithin-C was used to assess the anti-inflammatory activity. Interestingly, Urolithin-C efficiently reduced the expression of pro-inflammatory inducible enzyme (Cox-2), cytokines (IL-2, IL-6, and TNF-alpha) and increased the anti-inflammatory cytokine (TGF-beta1), compared to positive control diclofenac (DFC). Urolithin-C effectively abrogated the NF-κB p65 phosphorylation and its translocation to the nucleus as well. Most importantly, Urolithin-C efficiently suppressed the expression of pro-inflammatory genes and elevated the expression of anti-inflammatory gene.

Conclusion: Urolithin-C exhibited anti-inflammatory properties by regulating the expression of pro-inflammatory inducible enzyme, cytokines and the translocation of NF-κB p65 to the nucleus.

Keywords: anti-inflammatory, urolithin-C, cytokines, LPS, macrophage

Received: 9 May 2025
Accepted: 26 August 2025
Published: 9 September 2025

Graphical Abstract

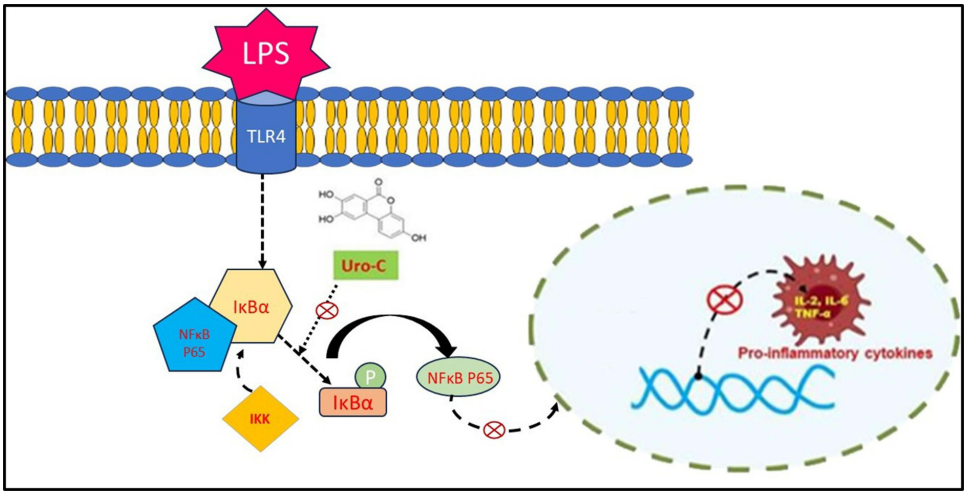

Introduction

Inflammation is a key cellular defense mechanism activated by harmful stimuli such as reactive oxygen species (ROS), pathogens, toxic compounds, radiation, and certain drugs.[1] Perhaps it is a vital phenomenon that eliminates tissue injuries by initiating the healing process.[2] Typically, during acute inflammatory conditions, there could be a cellular and molecular interaction that potentially regulates the impeding injury/infection that maintains tissue homeostasis.[3] However, uncontrolled acute inflammation turns into chronic inflammation implicated in the development and progression of tissue damage, thrombosis, stroke, cancer, diabetes, atherosclerosis, autoimmune and neurodegenerative disorders.[4] Numerous inflammatory pathways, including collective inflammatory mediators and regulatory mechanisms, impact the pathophysiology of the aforementioned chronic illnesses.[5] Inflammatory mediators are created when intracellular signaling pathways are triggered by microbial pathogens and tissue injury.[6] By interacting with the toll-like receptors (TLRs), IL-1 receptor (IL-1R), IL-6 receptor (IL-6R), and TNF receptor (TNFR), cytokines including interleukin-1β (IL-1β), interleukin-6 (IL-6), and tumour necrosis factor-α (TNF-α) mediated inflammation.[7] Key intracellular signaling pathways, including nuclear factor kappa-B (NF-κB), mitogen-activated protein kinase (MAPK), and Janus kinase-signal transducer and activator of transcription (JAK-STAT) pathways, are triggered when receptors are activated.[8–10] Tissue damage and inflammatory illnesses are caused by an overabundance of the inflammatory mediators TNF-α, IL-1β, and IL-6, in addition to iNOS (inducible nitric oxide synthase) and COX-2 (cyclooxygenase-2).[11–13]

However, inflammation regulation happens through macrophages, which detect external triggers to generate inflammatory mediators. Gram-negative bacteria activate macrophages through their lipopolysaccharide core elements, acting as an extensive *in-vitro* inflammatory trigger. The binding activation sequence between Toll-like receptor 4 (TLR4) activation often leads to the production of TNF-α, then TNF-α modulates TLR4 expression and signaling. The LPS binds to TLR4 and triggers NF-κB activation and mitogen-activated protein kinase signaling, which in turn triggers the upregulation of protein kinase B activation followed by pro-inflammatory mediators.[14,15] IκBα and p65 NF-κB are the inactive dimers upon phosphorylation (IκBα subunit), resulting in the release of p65 NF-κB (active), which then translocate into the nucleus which in turn activates the inflammatory genes transcription. The inhibitory proteins (IκBα) trap NF-κB in the cytoplasm of resting cells.[16–18] Research on anti-inflammatory drugs must figure out how to stop the signaling pathways. Nonsteroidal anti-inflammatory medications (NSAIDs), which include naproxen and ibuprofen with aspirin as a frequent companion, are a major component of the current anti-inflammatory therapeutic strategies.[19,20] Due to gastrointestinal, renal and cardiovascular complications during prolonged NSAID use, patients need more protective alternatives that function effectively.[21,22] Curcumin, colchicine, resveratrol, capsaicin,

epigallocatechin-3-gallate (EGCG), and quercetin are examples of naturally occurring manmade chemicals that help prevent the side effects of anti-inflammatory medications.[23]

The group of tannins called ellagic acid (EA) are produced when the human digestive tract hydrolyses ellagitannins (ETs), which are present in fruits, nuts, and seeds. The gut microbiota further transforms EA into other types of Urolithin derivatives (A, B, C, D, M-5, M-6, and M-7). Because they may be found in pomegranates as well as other fruits and nuts including strawberries, raspberries, grapes, walnuts, and chestnuts. The antioxidant and anti-inflammatory properties of natural polyphenols, particularly ellagitannins (ET) and ellagic acid (EA), are of interest to researchers.[24,25] The poor rate of absorption of these chemicals in the body limits their therapeutic potential. In addition, the role of Urolithin-C on inflammation is little understood, but the pharmacological characteristics and anti-inflammatory effect of Urolithins A and B were well established.[26–28] For instance, Urolithin A pacifies the production of pro-inflammatory cytokines such as TNF-α, IL-6, and IL-1β and inhibits the NF-κB signaling pathway by avoiding the phosphorylation of NF-κB p65. In addition, Urolithin A also regulates the MAPK pathways (ERK1/2 and p38).[29,30] While Urolithin B exhibits anti-inflammatory properties by desensitizing the NF-κB, JNK (Jun N-terminal Kinase), and ERK (Extracellular signal-regulated kinase) pathways.[31] As far as Urolithin C is concerned, anti-inflammatory effect was studied only in the framework of neuroinflammation and type I diabetes. None of the studies available on the anti-inflammatory action of chemically synthesized Urolithin-C on LPS induced inflammation in macrophages. Therefore, this study aims to synthesize Urolithin-C in-house and evaluate its anti-inflammatory potential in LPS-stimulated RAW 264.7 macrophages, focusing on its effect on key inflammatory mediators and signaling pathways, particularly NF-κB.

Materials and Methods

Chemicals and Reagents

In the current study, the reagents used were of superior quality and purchased from certified suppliers. 2-Formyl phenyl boronic acid, K_2CO_3 (Potassium Carbonate), 2-bromo-1-iodo-4-methoxybenzene, THF (Tetrahydrofuran), $PdCl_2(PPh_3)_2$ [dichloro bis (triphenylphosphine) palladium (II)], EtOAc (Ethyl acetate), BBr_3 (Boron tribromide), HCl (Hydrochloric acid), Methanol, phosphate buffer saline (PBS), bovine serum albumin (BSA), egg albumin, and trypsin. RAW 264.7- Mouse monocyte/macrophage-like cell line (NCCS, Pune, India). DMEM (Dulbecco's Modified Eagle Medium) with high glucose medium, Fetal Bovine Serum D-PBS, LPS from E. coli, DMSO (dimethyl sulfoxide), MTT (3-(4, 5-dimethylthiazol-2-yl)-2, 5-diphenyltetrazolium bromide), Antibiotic-Antimycotic solution-100x, Trypsin, EDTA, Tween-20, Diclofenac sodium, Primers-Mouse TNF-alpha, Cox-2, NF-κB, IL6, TGF-beta1 and GAPDH (glyceraldehyde-3-phosphate dehydrogenase), RNAiso plus-Total RNA extraction reagent, TB Green Premix Ex Taq II (Tli RNase H plus), Primer script RT reagent kit (Perfect Real Time), DEPC (Diethyl Pyro carbonate), RayBio Mouse IL-2 ELISA Kit, RayBio Mouse TNF-alpha (Tumor Necrosis Factor alpha) ELISA Kit, RayBio Mouse TGF-beta 1 (Transforming Growth Factor beta-1) ELISA Kit, Mouse IL6 ELISA Kit, Elabscience Mouse PTGS2/Cox-2 ELISA Kit, PE anti NF-κBp65 antibody, Poly-L-Lysine, Fixative solution, DAPI (4',6-diamidino-2-phenylindole) (hydrochloride), NF-κBp65 (F6) FITC (Fluorescein Isothiocyanate) antibody. The chemicals were obtained from Invitrogen (India) and Sigma Aldrich (USA).

Urolithin-C Synthesis

Urolithin-C was synthesized by following the previously described method of Tetrahedron,[32,33] in brief, with a slight modification of the Suzuki-Miyaura coupling reaction and copper-catalyzed cyclization method. All the spectral and physical properties of Urolithin-C matched with literature values.[34–36]

Synthesis of 6-(2-Bromo-4-Methoxyphenyl) Benzo[D] [1,3] Dioxole-5-Carbaldehyde (3)

2-Formylphenylboronic acid (1.0 equivalent), 2-bromo-1-iodo-4-methoxybenzene (2.0 equivalents), and 5 mol% bis-triphenylphosphine palladium (II) dichloride ($PdCl_2$ $(PPh_3)_2$) were combined in 5 mL of tetrahydrofuran (THF) in a reaction vessel. Agitation of the reaction mixture was done at room temperature, maintaining an inert environment. Using a syringe, a solution of 2 N K_2CO_3 (potassium carbonate) was gradually added to the reaction, causing the mixture to become brown red. Then the reaction mixture was kept stirring overnight at room temperature while utilizing thin layer chromatography (TLC) to track its development. Ethyl acetate (EtOAc)

was used to extract the mixture after the reaction was quenched with water. Finally, preparative thin layer chromatography was employed and EtOAc/hexane was used to purify the crude product. 65% brown oil: b.p. 128–131 °C, Rf 0.52 (10% EtOAc/Hexane). IR (KBr): λ_{max} 2902, 2852, 1674, 1606, 1478, 1239, 1039 cm^{-1}.

Synthesis of 3 Methyl 6-(2-Bromo-4-Methoxyphenyl) Benzo[D] [1,3] Dioxole-5-Carboxylate (4)

After adding pyridine (5 mL) and water (15 mL) to the solution of 2'-bromo-4-methoxy-(1,1'-biphenyl)-2-carbaldehyde (3) (1.0 equivalent), $KMnO_4$ (2.0 equivalent) was added at room temperature. The reaction mixture was then refluxed at 100–160 °C until the starting material was fully oxidized. The reaction mixture was then allowed to cool to room temperature before being acidified with 2 N HCl to produce a white precipitate and recrystallized using a 1:4 ratio of ethyl acetate (EtOAc) to hexane to produce biaryl carboxylic acid. The obtained product was dissolved using 25 mL of dichloromethane (CH_2Cl_2) in a round-bottom flask. Three drops of oxalyl chloride were gradually added to this carboxylic acid and dimethylformamide (DMF) solution that had already cooled. The obtained yellow residue was concentrated under low pressure after being agitated for two hours at 0 °C. At room temperature, 25 mL of methanol was used to esterify the residue. Ethyl acetate (EtOAc) was used to extract the reaction after it had been quenched with water. The residue was obtained by washing the organic layer with brine, drying it with anhydrous sodium sulphate (Na_2SO_4), and then concentrating it under reduced pressure. Dark red solid (52%): R_f 0.21 (10% EtOAc/Hexane). m. p. 84–86 °C. IR (KBR): λ_{max} 2952, 2908, 1724, 1604, 1472, 1242, 1034, 855 cm^{-1}.

Synthesis of 3-Methoxy-6H- [1,3] Dioxole [4',5':4,5] Benzo [1,2-C] Chromen-6-One (5)

TMEDA (1.0 equivalent) was added to a mixture of methyl 6-(2-bromo-4-methoxyphenyl) benzo[d] [1,3] dioxole-5-carboxylate (4) (1.0 equivalent), CuTC (0.5 equivalent), and K_2CO_3 (0.5 equivalent) in deionized water (2 mL) in a 100 mL round-bottom flask. The reaction mixture was then heated to 300 °C for 10 minutes, and thin-layer chromatography (TLC) was performed to follow the reaction. Following completion, the solution was rinsed with 100 mL of EtOAc and filtered through silica gel. A pale-yellow solid was obtained by removing the solvent under low pressure; this material was further refined using TLC (EtOAc/Hexane) to get the product. Brown solid (35%): R_f 0.39 (CH_2Cl_2/Hexane 50%). m. p. 117–1190 °C. IR (KBR): λ_{max} 2919, 2852, 2152, 1718, 1611, 1478, 1268, 1034, 935 cm^{-1}.

Synthesis of 3,8,9-Trihydroxy-6H-Benzo[C]chromen-6-One (Urolithin-C) (6)

Methyl ether of Urolithin-C (1.0 equivalent) was cooled to 0 °C in an aromatic environment, and boron tribromide (BBr_3) was gradually supplemented to the mixture and later the mixture was acidified with 2 N HCl solution. The product was then extracted using ethyl acetate (EtOAc), and the crude product was purified by washing thoroughly with hot ethyl acetate, methanol, and water. Filtered and used a variety of methods to verify the final product's purity. Light tan color solid, yield 52%, R_f 0.22 (90% Hexane/EtOAc); m. p. 328–332 °C. IR (λ_{max}): 3340, 3156, 1701, 1615, 1460 and 1282 cm^{-1}. ^{1}H NMR (400 MHz, DMSO-d6): δ 10.39 (br s, 1H), 10.16 (br s, 1H), 10.12 (br s, 1H), 7.85 (d, 1H), 7.49 (s, 1H), 7.41 (s, 1H), 6.81 (dd, 1H), 6.69 (d, 1H). ^{13}C NMR (100 MHz, DMSO-d6): δ 161.2, 159.3, 154.2, 152.4, 147.3, 129.9, 125.6, 115.3113.8, 112.2, 111.1, 107.7, 104.4. ESI m/z (%): 244 (12). Anal. Calcd for $C_{13}H_8O_5$: C, 63.94; H, 3.30. Found: C, 63.92; H, 3.34%.

Thin Layer Chromatography (TLC)

The product obtained was combined with 10% methanol and DCM (dichloromethane) and spotted on silica-plated aluminum sheets. A chromatogram was then created by means of a mobile phase consisting of 1% ethyl acetate and n-hexane. By visualizing the spot in an iodine chamber, the generated chromatogram was found.[34] With a retardation factor (Rf) value of 0.3 cm, the first reaction intermediate was seen. The final product, which had undergone acidification, bromination, and 2 N HCl, had an Rf value of 0.2 cm.

High-Performance Liquid Chromatography (HPLC)

HPLC was performed by loading 20 µL of the synthesized Urolithin-C through a 250×4.6 mm C-18 column (Agilent Technologies system in Santa Clara, California). A constant flow rate of 1 mL/minute was maintained. Water, acetonitrile, and 0.1% trifluoroacetic acid (TFA) were used in the gradient elution process.[35]

Nuclear Magnetic Resonance Spectroscopy (NMR)

The protons of synthesized Urolithin-C were identified and confirmed by using ^{1}H NMR. After being dissolved in dimethyl sulfoxide (DMSO), the synthesized Urolithin-C was run through an NMR spectrometer set to 400 MHz for proton frequency. The many carbon atom habitats inside a molecule were represented by peaks in the ^{13}C NMR spectra, which were used to clarify the structure of molecules. Urolithin-C was dissolved in DMSO and subjected to analysis using an NMR spectrometer set to run at a proton frequency of 400 MHz, much like in ^{1}H NMR. A Bruker 400 MHz device (Bruker, Bremen, Germany) was used to record NMR spectra.[32,33]

Fourier Transform Infrared Spectroscopy (FTIR)

The active functional groups found in the synthesized Urolithin-C were examined by the FTIR analytical method. A Shimadzu FTIR-8400 spectrometer was used to determine the FTIR spectra at wave numbers ranging from 600 to 4000 cm^{-1}.[36]

Liquid Chromatography Mass Spectrometry (LC-MS)

The analytes included in the synthesized Urolithin-C were identified and quantified using LC-MS. The Micro Mass Quattro Micro API (LCMS) from Waters was used to obtain the mass data. A 50×4.6 mm WATERS X Bridge C-18 column with a particle size of 3.5 µ was used for the chromatographic separation. At 1.2 mL/minute, the flow rate was kept constant. A solvent system including 0.1% formic acid, water, and acetonitrile was used to carry out gradient elution.[37]

Anti-Inflammatory Activity (*in-vitro*)

Assay for Membrane Stabilization

The previously mentioned method was used to quantify the membrane stabilization activity.[38] Nine milliliters of 10 mM PBS (pH 7.4) were added to 1 mL of human red blood cells. For 1 hour at 37 °C, 1 mL diluted blood sample was exposed to varying doses of 0–25 µg of Urolithin-C. 9 mL of ice-cold 10 mM PBS (pH 7.4) was added to stop the hemolytic process. The samples were centrifuged at 37 °C for 10 minutes at 1500 rpm. A positive control was provided by Triton-X100. By measuring and comparing the quantity of hemoglobin produced in the sample supernatant at 540 nm, the degree of hemolysis was determined. The following formula was used to get the hemolysis percentage:

Hemolysis inhibition percentage = 1-test sample absorption/control absorption × 100.

Protein Denaturation Assay

The protein denaturation test was carried out with previously published procedures.[39] Urolithin-C doses ranging from 0 to 25 µg were combined with 4.78 mL of phosphate-buffered saline (PBS) and 0.2 mL of 1% bovine serum albumin and egg albumin to create a reaction mixture. Aspirin served as a positive control. After being incubated at room temperature for 15 minutes, the reaction mixture was heated for 5 minutes in a water bath that was maintained at 70 °-C. A spectrophotometer was used to measure the absorbance of turbidity at 660 nm after the fluid containing tubes had cooled. The percentage of denaturation inhibition was calculated using the formula below:

% inhibition of denaturation = 1-test sample absorbance/control absorbance × 100.

Protease Inhibition Study

Inhibition of protease was quantified using a method.[40] In a dry, clean test tube, Urolithin-C (0–25 µg) was added, and it was allowed to incubate at room temperature for 5 minutes. 0.06 mg of trypsin and 1 mL of 20 mM Tris-HCl buffer (pH 7.4) were added to the reaction mixture. After adding 1 mL of 0.8% (w/v) casein, the reaction was sustained for

20 minutes. To stop the reaction, 2 mL of 70% perchloric acid was added and centrifuged the tubes for 10 minutes at 1500 rpm. The supernatant was collected and the absorbance was measured at 210 nm.

Molecular Docking Studies

The protein (PDB ID: 2PTN) and the chemical Urolithin-C were docked into the active region of the protein using Auto Dock Vina. The chemical structure of the substance was achieved from the PubChem database using the appropriate 2D orientation. Furthermore, ChemBio3D was used to minimize the molecule's energy. Following energy minimization, the ligand molecule was used as input for Auto Dock Vina to carry out the docking simulation. The Protein Data Bank provided trypsin's crystallographic structure (PDB ID: 2PTN). All heteroatom coordinates and water molecules were replaced with hydrogens, Kollman charges, and the absent C-terminal oxygen. In order to only accept receptor files devoid of non-integral charge residues, the Auto Dock 4.2 program was developed. The relevant residue from the protein structure was then eliminated, utilizing Auto Preparation of Target Protein File to create the target protein files. Auto Dock 4.2 and MGL tools 1.5.6.[41,42]

Anti-Inflammatory Activity of Urolithin-C on RAW 264.7 Cell Lines

Cell Culture

The RAW 264.7 (mouse monocyte/macrophage cell line) was acquired from NCCS in Pune, India. The cells were cultivated in Dulbecco's Modified Eagle Medium (DMEM) with high glucose and 4 mM L-glutamine adjusted to contain 1.5 g/L sodium bicarbonate. They were also supplemented with 10% fetal bovine serum (FBS) and 1% antibiotic-antimycotic solution in an atmosphere of 5% CO_2, 18% O_2, and 37 °C in a CO_2 incubator. They were sub-cultured every two days. RAW 264.7 cells were given the passage number P36 for the current study. Cells were detached from the plate surface using a solution of 0.01% EDTA and 0.025% trypsin (in D-PBS) after the density reached 80%.

MTT ((3-(4, 5-Dimethylthiazol-2-Yl)-2, 5-Diphenyltetrazolium Bromide) Assay

The cytotoxicity of Urolithin-C on RAW 264.7 cells was assessed by the MTT test.[43] A 96-well plate was plated with 15,000 cells in 200 µL of the suitable medium. Then the cells were added with various doses of Urolithin-C (12.5, 25, 50, 100, and 200 µg/mL). The medium containing LPS (1 µg/mL) was kept for 2 hours to produce inflammation. The cells were then cultivated for 24 hours at 37 °C with 5% CO_2. Cells treated with LPS were used as the positive control, whereas cells not treated with LPS were considered as the negative control. Cells were exposed to 100 µL of MTT (0.5 mg/mL) and 3 hours incubation was done at 37 °C. Formazan crystal was dissolved in 100 µL of dimethyl sulfoxide (DMSO). The resulting purple solution was measured at 570 nm using a microplate reader (ELZ-800, Biotek, USA). Cells fed just DMEM were thought to be completely viable. Cell viability as a percentage was calculated using the following formula:

Cell viability percentage = [absorbance of treated cells/absorbance of untreated cells] * 100.

Evaluation of Cell Morphology

For RAW 264.7 morphological alterations, cells were evaluated after being treated with Urolithin-C at varying dosages from 12.5 µg/mL to 200 µg/mL for 24 hours at 37 °C. An Inverted Biological Microscope (CKX-41, Olympus) and a camera were used to view and record cells at a 20x magnification and a 200 µM scale using MICAM software.

Quantitative Estimation of Inflammatory Cytokines by Enzyme-Linked Immunosorbent Assay (ELISA)

A 6-well plate containing 0.5×10^6 cells/mL of RAW 264.7 cells were treated for 48 hours to promote cell adhesion and achieve the necessary cell density. Stimulated the cells for 2 hours with 1 µg/mL of LPS, then using 25 µg/mL of Urolithin-C, incubation was done for 24 hours. The LPS (1 µg/mL) treated cells were used as a positive control, and for the negative control, cells alone (without LPS treatment) were used. Cells treated with diclofenac (1 mM) and LPS (1 µg/mL) were considered as the positive controls. Following a 24-hour treatment period, the supernatant was removed and given a 1x PBS wash. The cells were lysed with 0.1% phosphate-buffered saline with Tween 20 (PBST) buffer for

30 minutes on ice. The cells' monolayer was then scraped off using a cell scraper, and the whole contents were moved to a sterile Eppendorf tube. At 4 °C, the whole suspension was centrifuged for 10 minutes at 10,000 rpm. The lysate supernatant was collected and used for the ELISA, by following the manufacturer's instructions, the levels of Cox-2, IL-2, IL-6, TGF-beta1, and TNF-α in the supernatants were quantitatively determined using the mouse ELISA kit IL-2, IL-6, TGF-beta1, and TNF-alpha (Ray Biotech Labs, Peachtree Corners, GA) and Cox-2 (Elabscience, Texas, USA). Following treatment of the stop solution, a microplate reader (ELX-800, BioTek, USA) was used to quantify the expression levels of Cox-2, IL-2, IL-6, TGF-beta1 and TNF-α at 450 nm.

Nuclear Translocation Analysis of NF-κB p65 Using the Confocal Laser Scanning Microscopy (CLSM) Technique

Coated the 35 mm glass bottom dishes with 500 µL of Poly-L-Lysine solution for 15 minutes and washed the dishes with 1 mL of PBS to remove the excess solution. Cells were cultured at a density of 0.5×10^6 cells/2 mL in each well of a plate, and the cells were stimulated for two hours with 1 µg/mL of LPS. The cells were incubated for 24 hours after being treated with 25 µg/mL of Urolithin-C and controls in 1 mL of culture media. The cells that received no treatment were regarded as negative controls, cells that were stimulated with 1 µg/mL of LPS were regarded as positive controls, and cells that received LPS (1 µg/mL) treatment and then 1 mM of diclofenac were regarded as positive controls. After the incubation, the medium was taken out of each well and PBS was used for washing. The cells were fixed and permeabilized for 30 minutes at room temperature using 500 µL of fixative solution (4% paraformaldehyde in PBS). After removing the PBS, 500 µL of blocking solution (1x PBS with 5% FBS and 0.3% Triton-X100) was added, and the mixture was incubated for an hour at room temperature. After fully aspirating the solution, the diluted NF-κB p65 antibody conjugate (1:500) was added together with fluorescein isothiocyanate (FITC). After washing the specimens three times with 1x PBS, the plates were kept in the dark at 4 °C for a whole night. The specimens were then incubated in antibody dilution buffer for 1–2 hours at room temperature in the dark. It was rinsed three times for 5 minutes each with 1x PBS, and before imaging, the cells were counterstained with 500 µL of diluted 4',6-diamidino-2-phenylindole (DAPI) stain solution with 1x PBS Solution (1 µg/mL) for 10 minutes without light. Using a filter cube, the cells were seen using the ZEISS LSM 880 Fluorescence Live Cell Imaging System (Confocal Microscopy) with excitation and emission of 358 nm and 461 nm for DAPI and 495/519 nm for FL1 channel. Photographs were taken and captured with ZEN Blue Software. The software Image J (FIJI) was used to analyse the captured pictures.

Gene Expression Study by RT-qPCR

Total RNA extraction and qRT-PCR were carried out with minor alterations as previously outlined.[44] The cells were cultivated on a 6-well plate at a density of 0.5×10^6 cells/mL of RAW 264.7. The cells were stimulated with 1 µg/mL of LPS for two hours, and treated with 25 µg/mL of Urolithin-C and allowed to incubate for 24 hours. An untreated cell were used as a negative control, cells treated just with LPS (1 µg/mL) as a positive control, and cells treated with LPS and 1 mM diclofenac as the positive control. Once the treatment was completed, rinsed with 500 µL PBS and trypsinated with 500 µL of trypsin-EDTA. The cells were then incubated for 3–4 minutes at 37 °C, and centrifuged for five minutes at 300 x g at 25 °C and the cells were rinsed twice with PBS and 500 µL of RNAiso Plus reagent was added straight into the Eppendorf tube containing the lysed tissues and homogenized. Centrifuged the lysate for five minutes at 12,000 rpm at 4 °C, to the supernatant 200 µL of chloroform was added, and centrifuged the sample. To the aqueous phase added 500 µL of isopropanol and was centrifuged to collect the pellet. The pellet was resuspended in 1 mL of 75% ethanol. The RNA pellet was allowed to air dry at ambient temperature for 10 minutes and resuspended in 50 µL of water devoid of RNase. The RNA was kept for later use at 80 °C while the tubes were incubated in a water bath at 55–60 °C. Using a Nanodrop Spectrophotometer (Thermo Fisher Scientific, Waltham, MA, USA) set at 260 and 280 nm, the concentration and purity of total RNA were measured.

Synthesis of cDNA with the Prime Script RT Reagent Kit (Perfect Real Time)

The I Script cDNA synthesis kit for PCR amplification was purchased from Eurofins in Bangalore, and it was used to reverse-transcribe RNA into complementary DNA (cDNA). The TB Green Premix Ex Taq II (Tli RNase H plus, Takara)

was used in the Quant Studio3 system (Thermo Fisher) to perform the relative quantification of the gene expression. Table 1 contains a list of the primers used. The fluorescence is obtained via PCR cycling settings, which comprise a primary denaturation at 95 °C for 15 seconds, 40 cycles of denaturation at 95 °C for 20 seconds, annealing at 60 °C for 20 seconds, and extension at 95 °C for 20 seconds. Following the PCR protocol, the melt curve continually records fluorescence at 0.5 °C increments per minute from 65 to 95 °C. A Prime Script RT reagent kit was then used to perform qRT-PCR on the samples. 2 µL of cDNA, 10 µL of TB Green Premix Ex Taq II (2X), 0.8 µL of each forward and reverse primer (10 µM), 0.4 µL of Rox reference dye, and 6 µL of nuclease-free water made up each reaction mixture. Every sample was carried out twice, and the results were averaged. To evaluate the PCR's correctness, melting curves were produced. GAPDH was used as an endogenous internal control gene, and the expression levels of calibrator genes were measured using the 2−ΔΔCt technique. ΔCt values were computed as follows:

ΔCt = Ct (target gene) − Ct (housekeeping gene), and also

ΔΔCt = ΔCt (treatment) − ΔCt (control).

Table 1 Primers Used in the Current qRT-PCR Investigation Sequence

Name		Sequence	Gene Accessions No
mTNF-alpha	FP	GGTGCCTATGTCTCAGCCTCTT	NM_013693
	RP	GCCATAGAACTGATGAGAGGGAG	
mNfkB1	FP	GCTGCCAAAGAAGGACACGACA	NM_008689
	RP	GGCAGGCTATTGCTCATCACAG	
mIL6	FP	TACCACTTCACAAGTCGGAGGC	NM_031168
	RP	CTGCAAGTGCATCATCGTTGTTC	
mTGf beta1	FP	TGATACGCCTGAGTGGCTGTCT	NM_011577
	RP	CACAAGAGCAGTGAGCGCTGAA	
mCox2	FP	GCGACATACTCAAGCAGGAGCA	NM_011198
	RP	AGTGGTAACCGCTCAGGTGTTG	
mGAPDH	FP	CATCACTGCCACCCAGAAGACTG	NM_008084
	RP	ATGCCAGTGAGCTTCCCGTTCAG	

Statistical Analysis

Statistical analysis was done, and the results were presented as mean ± SD. Graph Pad Prism 5.0 (Graph Pad Software, Inc., San Diego, CA, USA) was used to compare individual parameters using a one-way ANOVA. The statistical significance of the p-value ($p < 0.05$) was established.

Results

Urolithin-C Synthesis

The four-step procedure used to synthesize Urolithin-C (6) is shown in Scheme 1. In the first step, biaryl carbaldehyde (3) was produced with a yield of roughly 70% when 2-formyl phenyl boronic acid (1) and 2-bromo-1-iodo-4-methoxybenzene (2) were combined with bis-triphenylphosphine palladium (II) dichloride ($PdCl_2(PPh_3)_2$) as a catalyst under basic conditions and tetrahydrofuran (THF) at room temperature. The second process included oxidizing biaryl carbaldehyde (3) using water, pyridine, and potassium permanganate. Additionally, it was esterified to create a biaryl carboxylic ester using methanol and dimethylformamide (4). In the third step, 3-methoxy-6H-[1,3] dioxolo [4',5':4,5] benzo [1,2-c] chromen-6-one (5) was formed by `

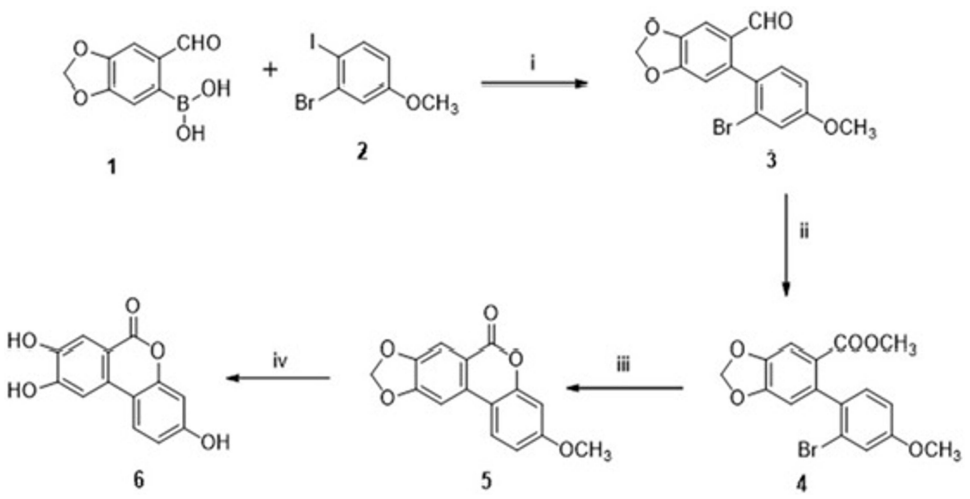

Scheme 1 Reaction Conditions: (i) $PdCl_2(PPh_3)_2$, THF, excess, K_2CO_3, RT. (ii) a. $KMnO_4$, Pyridine, H_2O, reflux, b. ($COCl_2$), Cat.DMF, CH_2Cl_2, CH_3OH. (iii) CuTC, TEMED, K_2CO_3, H_2O, 300 °C, 10 minutes. (iv) BBr_3, 2 N HCl.

combining biaryl carboxylic ester (4) with N,N,N',N' tetramethyl ethylene diamine and potassium carbonate at 300 °C with Copper(I) thiophene-2-carboxylate (CuTC). Compounds 3, 4, and 5's spectral and physical analyses agreed with values reported in the literature.[28,30–32] After the chemical (5) was demethylated with boron tribromide in the presence of dichloromethane and hydrochloric acid, Urolithin-C (6) was produced with a 52% yield.

Synthesized Urolithin-C Purification and Characterization

The purity of the synthesized Urolithin-C was assessed using TLC; a single spot of Urolithin-C was seen having the RF values of (retardation factor) 0.39 cm and 0.22 cm, respectively, for both first and second reaction intermittent (Figures 1A and B). Additionally, HPLC was used to assess the purity of Urolithin-C; a single sharp peak having the retention time of 10.902 minutes was noticed (Figure 2). ^1H and ^{13}C NMR were used to analyse the likely structure. Parts per million (ppm) were used to report the proton chemical shift (δ). ^1H NMR (400 MHz, DMSO-d6): δ 10.39 (br s, 1H), 10.16 (br s, 1H), 10.12 (br s, 1H), 7.85 (d, 1H), 7.49 (s, 1H), 7.41 (s, 1H), 6.81 (dd, 1H), 6.69 (d, 1H) (Figure 3). ^{13}C NMR (100 MHz, DMSO-d6): δ 161.2, 159.3, 154.2, 152.4, 147.3, 129.9, 125.6, 115.3, 113.8, 112.2, 111.1, 107.7, 104.4 (Figure 4). Using Fourier transform infrared (FTIR) spectroscopy, the potential functional groups of the synthesized Urolithin-C were determined. An outlying peak at wavelengths 3361–3326 cm^{-1} denotes the stretching of a polymeric hydroxyl group (O-H stretching). The free phenolic functional groups (O-H stretching) were the cause of the absorption peak at wavenumber 2994 cm^{-1}. Additionally, the existence of a ketone moiety is implied by C=O stretching at 1705 cm^{-1} and C=C stretching at 1620 cm^{-1}. A C=C bending

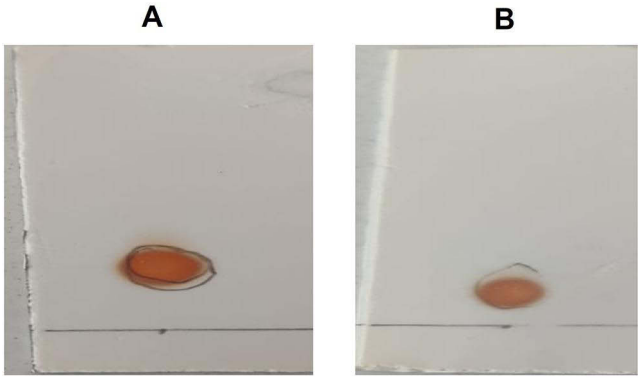

Figure 1 Chromatogram of Urolithin-C: (**A**) Chromatogram represents the retardation factor (RF) of 0.3 cm. (**B**) Chromatogram represents the retardation factor (RF) of 0.2 cm.

https://doi.org/10.2147/JIR.S539273

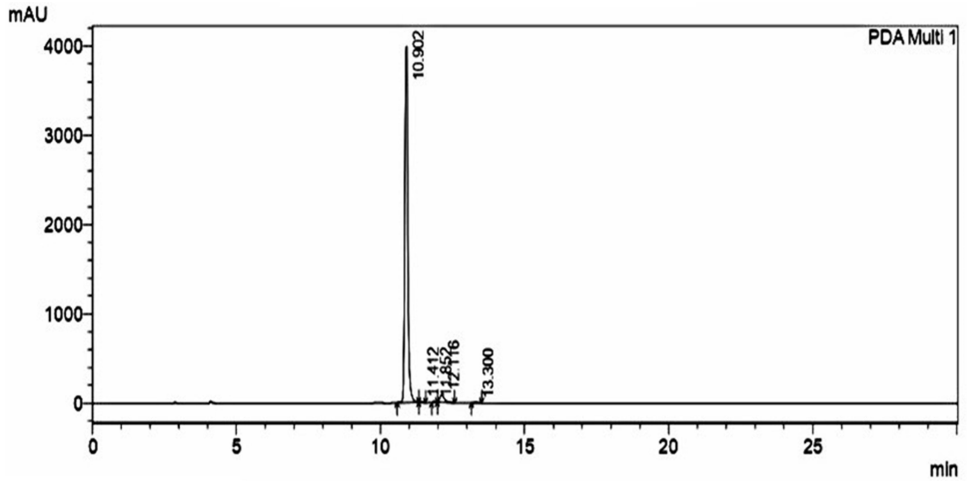

Figure 2 Urolithin-C HPLC chromatogram with a 10.902-minutes retention time.

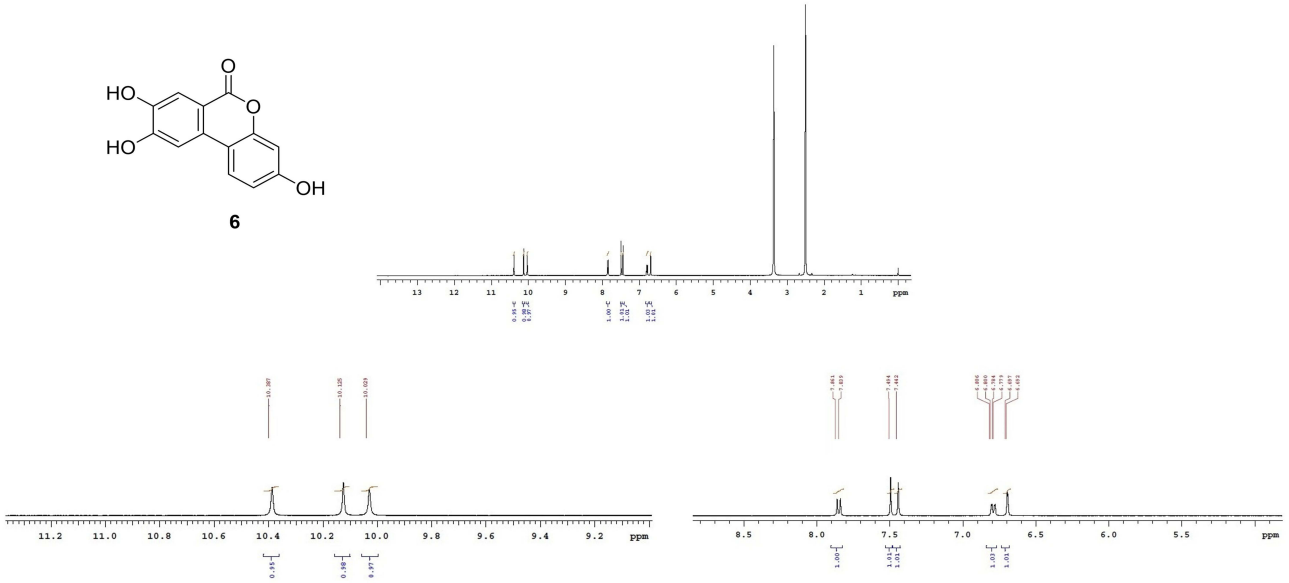

Figure 3 NMR spectra of Urolithin-C: ^{1}H NMR spectra of Urolithin-C, ^{1}H NMR spectra of Urolithin-C showing three peaks of hydrogen present in the hydroxyl group and ^{1}H NMR spectra of Urolithin-C showing five peaks of hydrogen present in Urolithin-C.

feature of the alkene moiety was shown in the region between 988 and 698 cm^{-1}, and this spectrum confirmed Urolithin-C's structure (Figure 5). Additionally, the mass data obtained using Liquid LC-MS (Figure 6) verified that the mass of the synthesized chemical was 244.53 g/mole with respect to the negative mode of m/z ratio.

Urolithin-C Exhibits Anti-Inflammatory Property

Interestingly, Urolithin-C prevented RBC membrane lysis, demonstrating its anti-inflammatory property through antihemolytic action (Figure 7A). Urolithin-C's anti-inflammatory property was further shown by the denaturation of egg albumin and bovine serum albumin (Figure 7B and C). Urolithin-C reduced the denaturation of egg and bovine serum albumin in a concentration-dependent fashion. Urolithin-C was shown to suppress protein denaturation at a percentage of 84.64% for egg albumin and 76.05% for bovine serum albumin, respectively, compared to 90% for the positive control aspirin. The main enzyme that neutrophils release during inflammation is serine protease, which is essential for tissue degradation during the inflammatory response. Thus, an inhibition of the protease (trypsin) was carried out. Curiously, Urolithin-C significantly reduced the protease

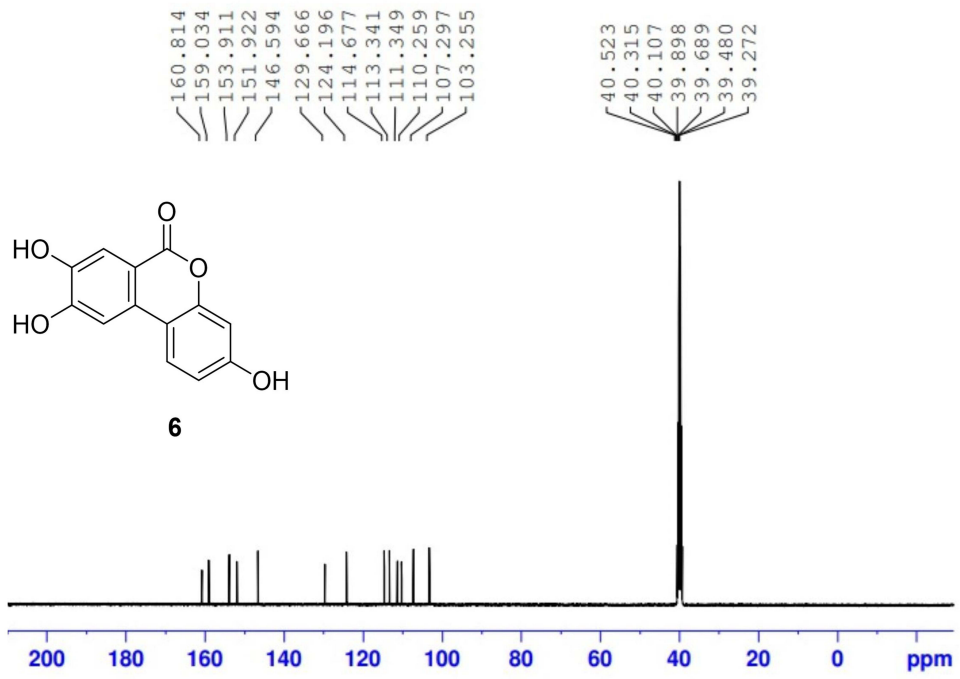

Figure 4 ^{13}C NMR spectra of Urolithin-C.

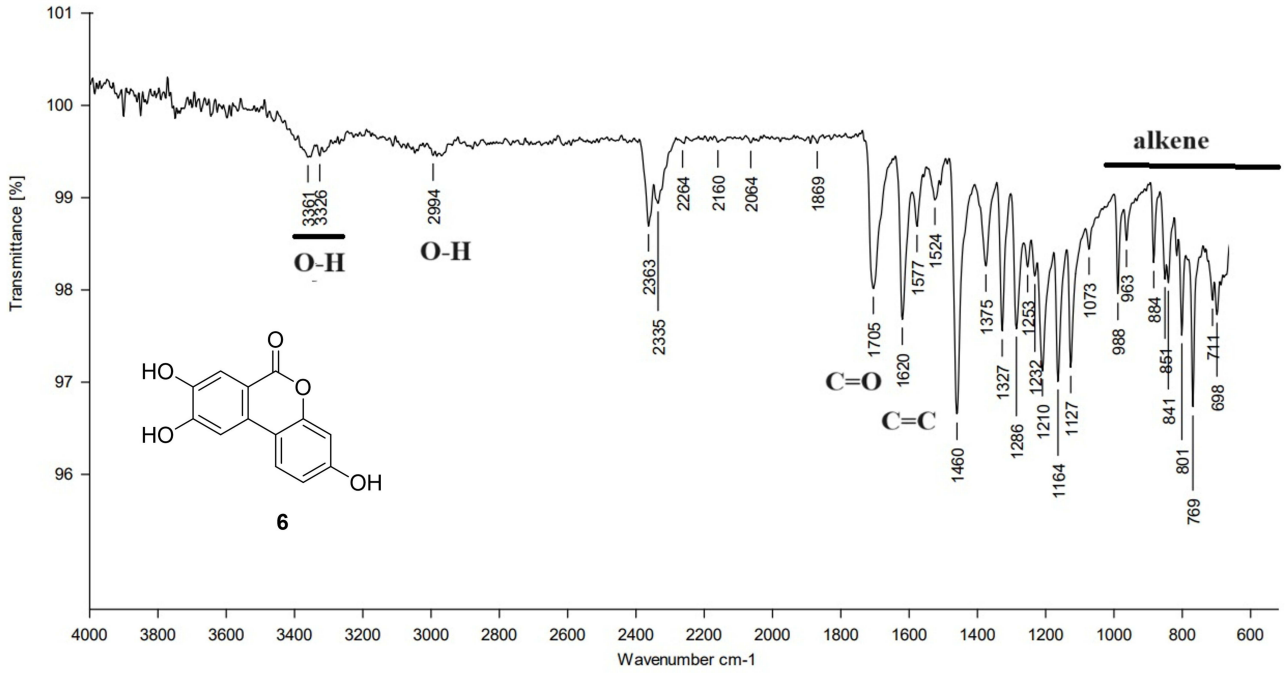

Figure 5 FTIR spectrum revealing Urolithin-C's functional groups.

activity in contrast to the positive control aspirin (Figure 7D). Protease inhibition percentages in Urolithin-C and positive control aspirin were reported to be 80% and 94%, respectively.

In Silico Effect of Urolithin-C

The interaction between the enzyme and inhibitor was investigated using molecular docking techniques. Urolithin-C showed a binding energy of −7.1 kcal/mol when it interacted with the trypsin enzyme (Figure 8). Urolithin-C engaged

https://doi.org/10.2147/JIR.S539273

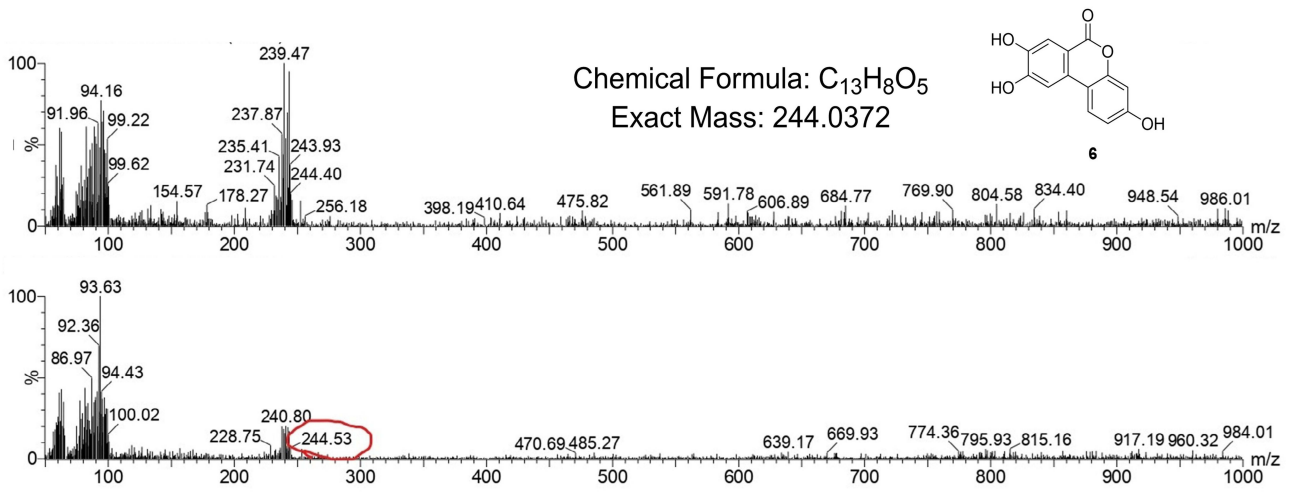

Figure 6 The molecular weight of Urolithin-C was determined using LC-MS Chromatography of Negative Modes. The molecular weight of the Urolithin-C was found to be 244.53 which is highlighted in red color.

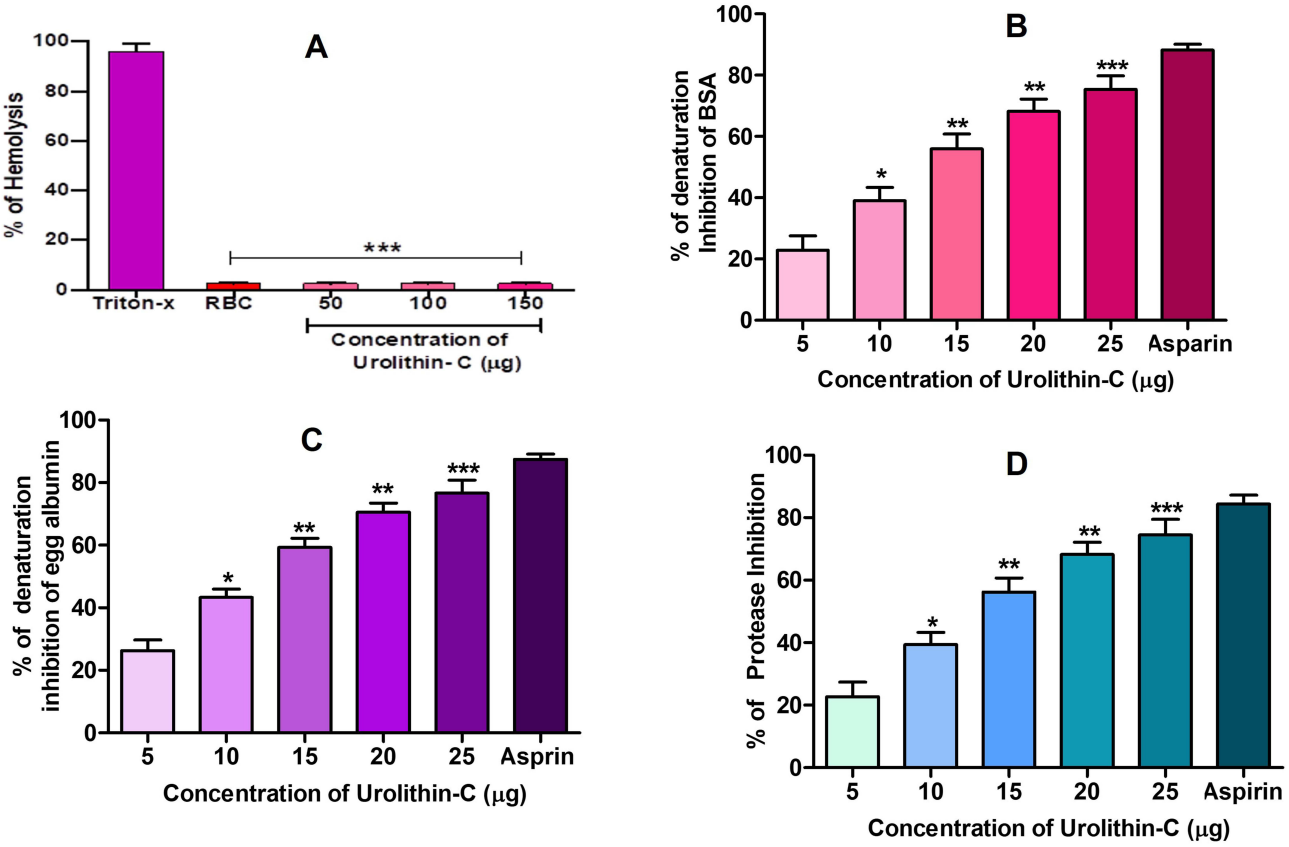

Figure 7 Urolithin-C's impact on protein denaturation (**A**) Direct hemolytic activity (**B**) percentage of BSA denaturation inhibition, (**C**) percentage of egg albumin denaturation inhibition, and (**D**) percentage of protease inhibition. The data are provided as mean ± SEM (n = 3) and are shown in average units/mg of protein. ** at $p \leq 0.01$, ***at $p \leq 0.001$ and * at $p \leq 0.05$.

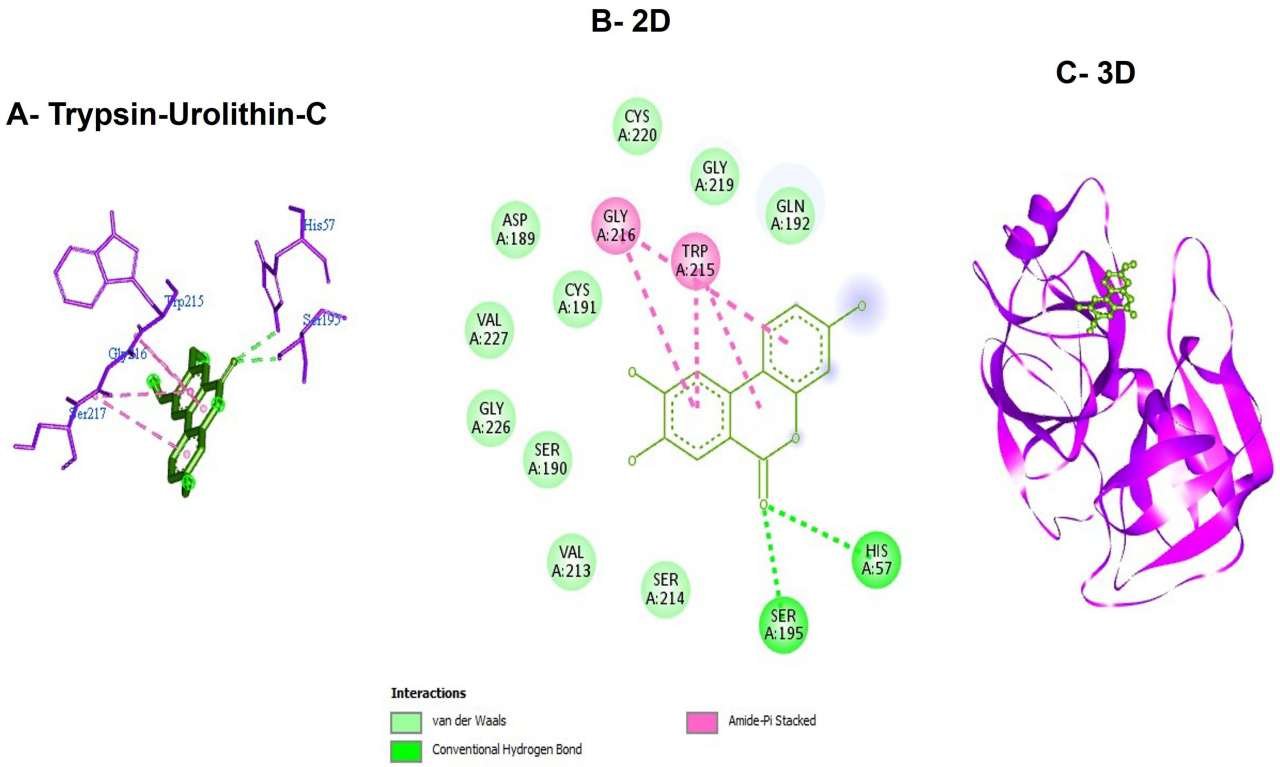

Figure 8 Trypsin- Urolithin-C interaction studies by molecular docking: (**A**) Trypsin - Urolithin-C Binding, (**B**) 2D (**C**) 3D image of binding of Urolithin-C on protein through hydrogen bonding (SER A:195 and HIS A:57) to inhibit the action of protein with a docking score of 7.1 kcal/mol.

with the conserved amino acid residues Ser195 and His57 at the active site via hydrogen bonding. Gly 216 and Trp 215 display amide-π stacking interactions with the ligand Urolithin-C. Therefore, Urolithin-C inhibited trypsin's activity.

Urolithin-C Exhibits Moderate Cytotoxicity in RAW 264.7 Cells

The MTT test was used to evaluate Urolithin-C cytotoxic effect on RAW 264.7 cells. During a 24-hour incubation period, the murine macrophage RAW 264.7 (Figure 9A) cells treated with a higher concentration (200 µg/mL) of Urolithin-C showed a cell viability rate of 58.55%. However, when RAW 264.7 cells were exposed to 1 µg/mL of LPS alone (positive control) showed a viability rate of 99.5%. It is to state that, at the concentration of 25 µg/mL, Urolithin-C was found to be safer as it showed 85.19% ofcell viability rate. Hence, 25 µg/mL of Urolithin-C was used for further mechanistic studies. Additionally, LPS-treated RAW 264.7 cells exhibited spindle-shaped pseudopodia, an indication of macrophage activation, while Urolithin-C maintained the rounded form of the pseudopodia (Figure 9B).

Urolithin-C Suppresses Cox-2, Pro-Inflammatory Cytokines and Stimulates Anti-Inflammatory Cytokines in LPS Treated RAW 264.7 Cells

To quantify inducible enzyme Cox-2 and expression of cellular pro/anti-inflammatory cytokines, IL-2, IL-6, TNF-alpha, and TGF-beta1 levels in LPS-stimulated RAW 264.7 cells, examined by ELISA. In the LPS-induced model, Urolithin-C suppressed the activity of Cox-2 and pro-inflammatory cytokines, including TNF-alpha, IL-2, and IL-6 (Figure 10A–10D). However, inducible enzyme (Cox-2) and the said cytokines were significantly expressed in cells treated with LPS (1 µg/mL) alone. Urolithin-C at 25 µg/mL has an anti-inflammatory impact in LPS-induced murine macrophages via suppressing inducible enzyme Cox-2 and cytokine expression. TGF-beta1, a cellular anti-inflammatory cytokine, was enhanced in RAW 264.7 treated cells induced by LPS (Figure 10E).

https://doi.org/10.2147/JIR.S539273

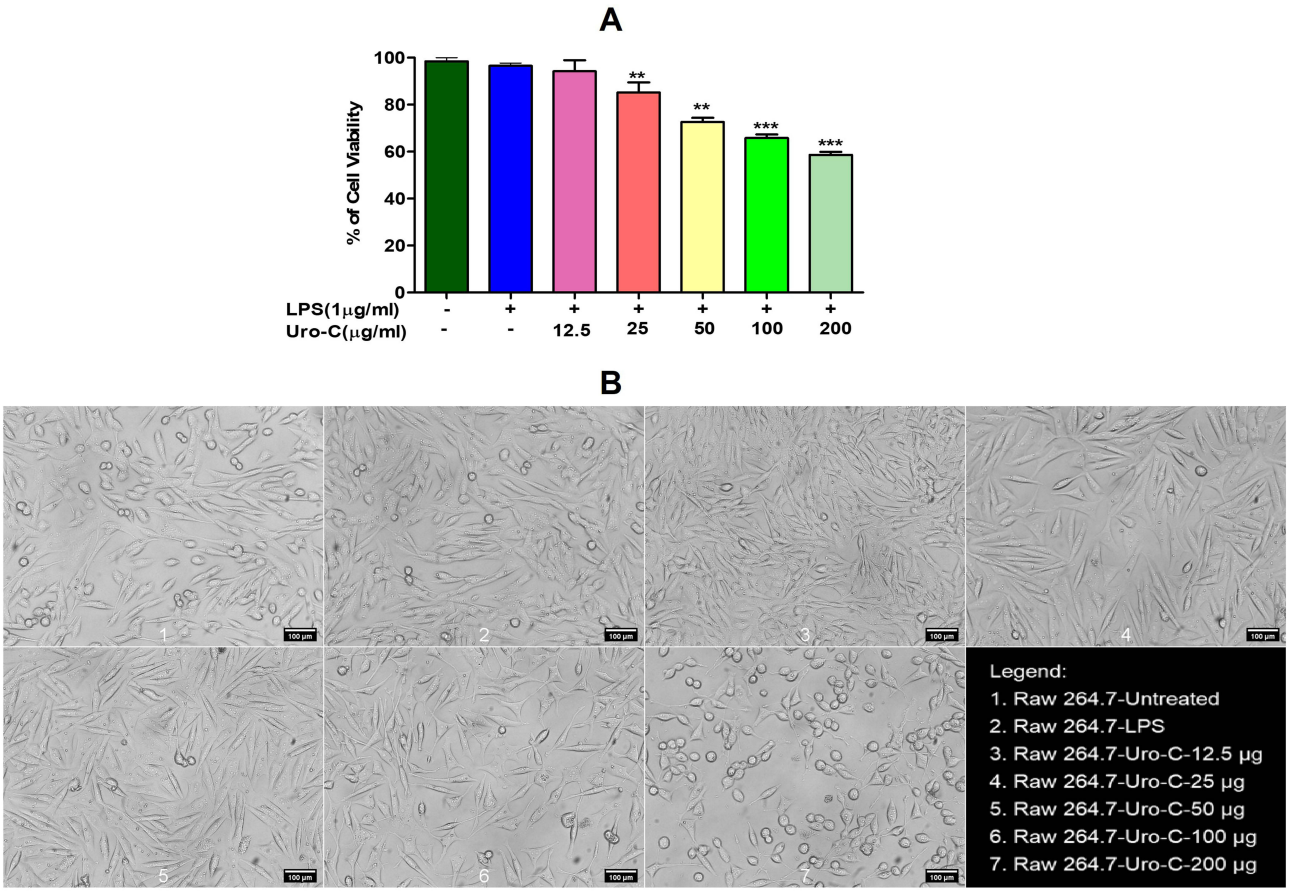

Figure 9 Urolithin-C's impact on RAW 264.7 cells: (**A**) RAW 264.7 cell viability percentage. After a 24-hour incubation period, RAW 264.7 cells were treated with different doses of Urolithin-C. (**B**) An inverted biological microscope was used to view the cell morphology. 200 μm is the scale bar. The mean ± SEM (n = 2) is used to express the results. ** at $p \leq 0.01$, *** at $p \leq 0.001$, and significance at $p \leq 0.05$.

Urolithin-C Regulates the Translocation of NF-κB

The regulatory effect of Urolithin-C on NF-κB translocation was investigated using a Confocal Laser Scanning Microscopy (CLSM) technique (Figure 11A). In the steady state, RAW 264.7 cells were devoid of p65 protein. As shown by the cells seen under the Fluorescence Live Cell Imaging System (Confocal Microscopy); instead, it translocated from the cytosol to the nucleus in response to LPS stimulation. However, this translocation was repressed by diclofenac (DFC) and Urolithin-C. Furthermore, Urolithin-C at a dose of 25 μg/mL in LPS (1 μg/mL) stimulated RAW 264.7 cells resulted in a 1.69±0.48 relative mean fluorescence intensity of NF-κB p65, while LPS (1 μg/mL) alone resulted in a 5.88±1.15 relative mean fluorescence intensity. Diclofenac (1 mM) was employed as a positive control for the investigation, resulting in a 3.76±0.86 relative mean fluorescence intensity of NF-κB p65 (Figure 11B). Overall, the findings revealed that the Urolithin-C anti-inflammatory effect could be due to the downregulation of NF-κB p65 expression.

Urolithin-C Upregulates Anti-Inflammatory Cytokine Gene Expression While Downregulating That of Pro-Inflammatory Cytokine Gene Expression

RT-PCR gene expression analysis revealed that the TGF-beta1 cytokine was successfully suppressed in LPS-treated RAW 264.7 cells, but relative gene translocation to the nucleus. The levels of TNF-alpha, Cox-2, NF-κB p65, and IL-6 genes were elevated. In LPS-induced RAW 264.7 cells, Urolithin-C at a concentration of 25 μg/mL efficiently suppressed pro-inflammatory cytokines while promoting anti-inflammatory cytokines. As a standard control for the current

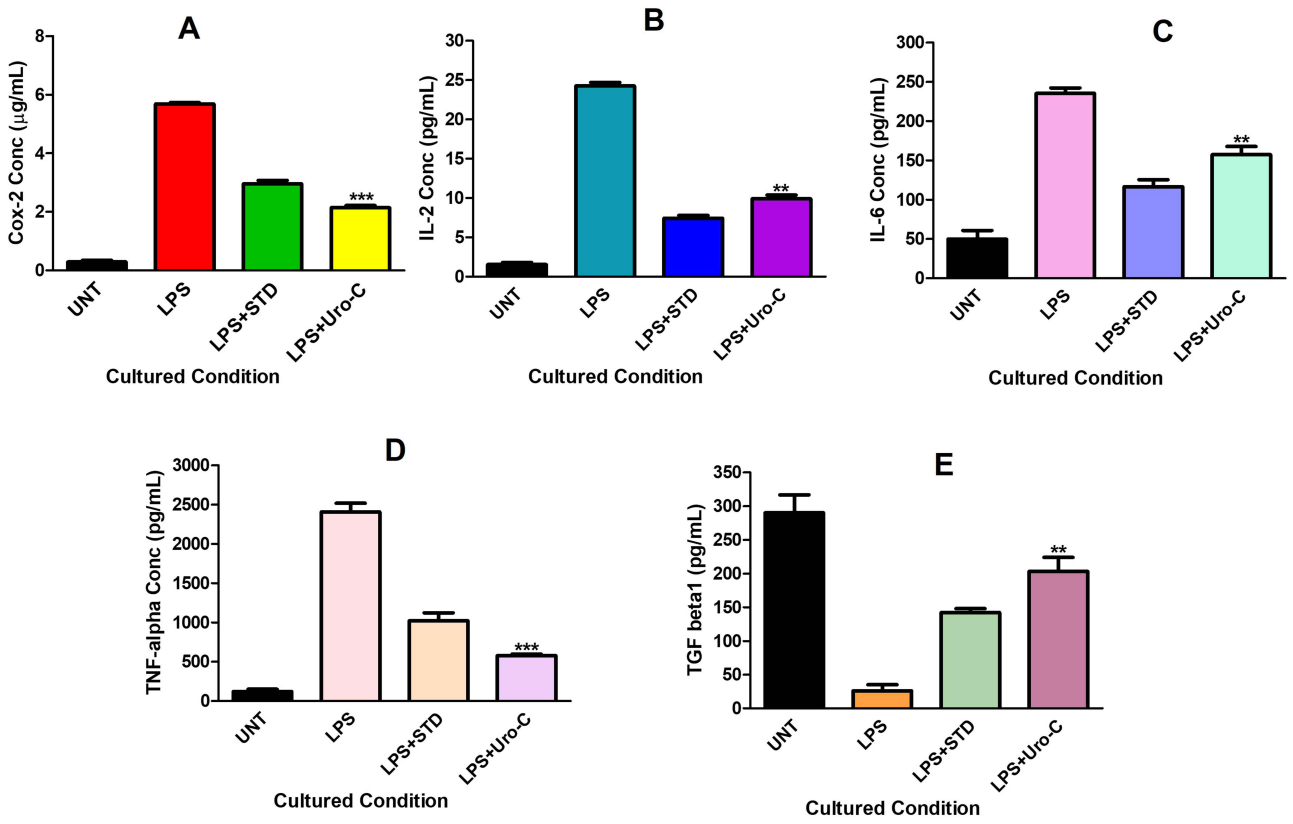

Figure 10 Urolithin-C's influence on pro/anti-inflammatory cytokines produced by LPS in RAW 264.7 cells: Following LPS, Positive control (DFC), and Urolithin-C (25 µg/mL) cell culture, ELISA was used to evaluate the production of (**A**) Cox-2, (**B**) IL-2, (**C**) IL-6, (**D**) TNF-α, and (**E**) TGF-β. The mean ± SEM (n = 2) is used to express the results. ** at $p \leq 0.01$ and ***at $p \leq 0.001$.

investigation, 1 mM DFC was utilized, which repressed the pro-inflammatory cytokines and stimulated the anti-inflammatory cytokines (Figure 12A–C).

Discussion

Inflammation is a physiological phenomenon; acute inflammation appears to be protective, while chronic inflammation results in severe tissue damage, thrombosis, cancer, diabetes, atherosclerosis, stroke, rheumatoid arthritis and neurodegenerative disorders.[45] Hence, inflammation becomes the fundamental target of deep attention in searching for novel anti-inflammatory molecules that regulate inflammation-induced pathogenesis.[46] Synthesized natural products via a chemical route may offer a potential therapeutic option in managing chronic conditions.[47] EA and ET are acted upon gut microbiota, resulted in the formation of Urolithin-C. It is thought that the health benefits of ET could be linked to these gut-produced Urolithin-C. Urolithin-C is not a common molecule in nature, although it may be found in plasma, urine, and the fecal matter of animals at amounts ranging from high nM to low mM. This study aimed to examine the impact of chemically synthesized Urolithin-C due to its restricted availability in a biological system.

Protein denaturation leads to an inflammatory response as altered proteins may be recognized as foreign by the immune system.[48] In addition, altered proteins, exposed to hidden antigens, that can trigger an immune response, resulting in tissue damage, arthritis and various severe pathogenesis.[49] Most importantly, anti-hemolytic agents and inflammation are interconnected, as lysed RBCs (red blood cells) released into the bloodstream act as damage-associated molecular patterns, or DAMPs, causes inflammation.[50] Pro-inflammatory cytokines, including IL-1β, TNF-α, and IL-6 are released as a result of hemolysis, along with other chemicals that promote tissue damage and inflammation.[51] Inflammatory mediator activation is prevented by compounds that stabilize the red blood cell membrane and shield it from harm in hot or hypotonic environments.[48,52] Interestingly, Urolithin-C prevented albumin denaturation and stabilized heat-induced RBC lysis, revealing

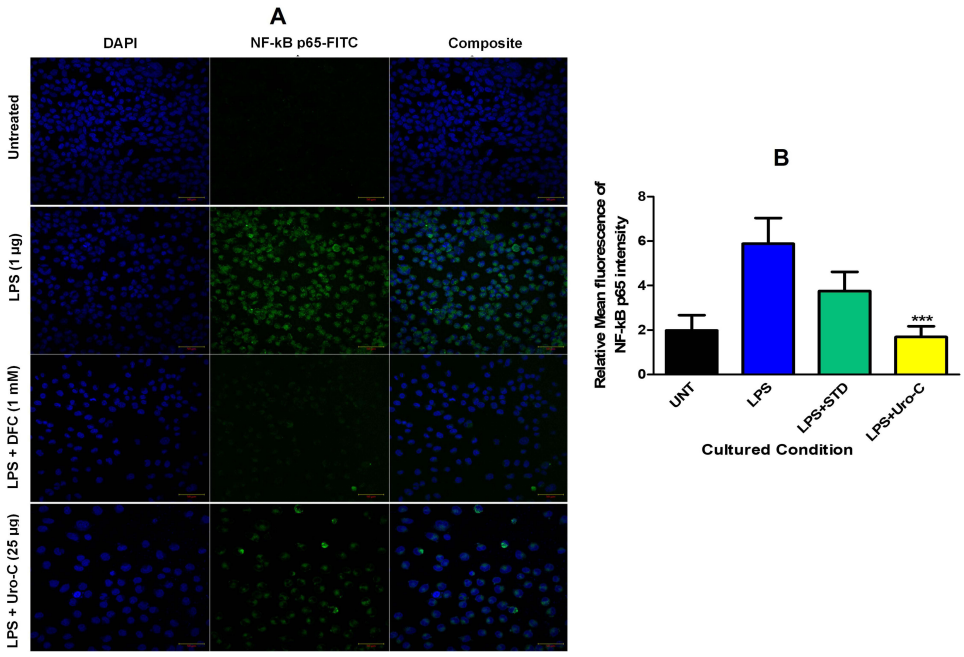

Figure 11 Effect of Urolithin-C on NF-κB translocation: (**A**) Microscopic image depicted the NF-κB p65-FITC expression in untreated, LPS alone and Co-treatment of LPS followed by DFC with 1mM or Urolithin-C with 25 µg/mL concentration on RAW 264.7 cells at the magnification of 40X at Blue and FITC channels. Cell nuclei are counter-stained with DAPI solution. (**B**) NF-κB p65 expression was observed in Untreated, LPS alone, DFC with 1mM and Urolithin-C with 25 µg/mL and 1 µg/mL of LPS pre-treatment treated RAW 264.7 cells after the incubation period of 24 hrs by Confocal microscopy. The results are expressed as mean ± SEM (n = 2). Significance at $p \leq 0.05$, *** at $p \leq 0.001$.

its anti-inflammatory properties. Research has demonstrated that by stabilizing the RBC membrane and preventing protein denaturation, plant extracts, saponins, hydroxyurea, l-glutamine, and nanoparticles including TAFE MgO NPs, TiO_2 NPs, and DHLE.$CoFe_2O_4$ NPs have an anti-inflammatory impact.[48,49,52,53]

The primary enzyme that neutrophils release, serine protease, is essential for both positively and negatively controlling the inflammatory process by influencing cytokine production and inducing receptor up regulation that affects the survival of cells.[54] Thus, a protease (trypsin) inhibition was done, and Urolithin-C effectively inhibited trypsin a serine protease, further strengthened its anti-inflammatory activity. Previous report revealed that the protease inhibition activity of plants extracts *Azadirachta indica, Camellia sinensis, Terminalia chebula, Piper nigrum*, green synthesized nanoparticles such as TAFE MgO NPs, TiO_2 NPs and DHLE. $CoFe_2O_4$ NPs showed significant protease inhibition activity.[47,48,52,55] Furthermore, an in silico molecular docking investigation verified Urolithin-C's ability to block trypsin. Since molecular docking gives fundamental information on binding energy, pattern, and affinity, it is critical in the initial phases of drug design. Urolithin-C's docking experiments with trypsin revealed a higher binding energy of −7.1 kcal/mol. Through hydrogen bonding, Urolithin-C reacted with the amino acid in the active site.

White blood cells (leukocytes, lymphocytes) and many other inflammatory cells may get activated throughout the inflammatory process. In many inflammatory diseases, macrophages are able to trigger the generation of pro-inflammatory mediators.[56] Gram-negative bacteria's cell wall contains lipopolysaccharide (LPS), which is a potent inducer of monocytes to macrophages during inflammation. It also triggers the production of proinflammatory mediators and activates immune cells via the toll-like receptor 4 (TLR4) chain.[57] Changes in cell size and cytoplasmic expansion are hallmarks of macrophage activation.[58] In order to apply a safer dosage (sub-toxic concentration), the cytotoxic impact of synthesized Urolithin-C was detected in murine monocyte/macrophage RAW 264.7 cells. The MTT test was used to assess the viability of RAW 264.7 cells at different Urolithin-C doses.[43] The safer dose was identified as 25 µg/mL.

The production of the inflammatory response is thought to involve several important mechanisms, including the activation of pro-inflammatory cytokines (IL-1, IL-6, IL-8, IL-12, IL-17, IL-18, TNF-α, IFN-γ, and IL-2).[59] Its release, however, is associated with both acute and chronic inflammation, promoting prostaglandin production and triggering the acute-phase response. Thus, we also looked into Urolithin-C's regulatory effects on cytokines that promote and inhibit

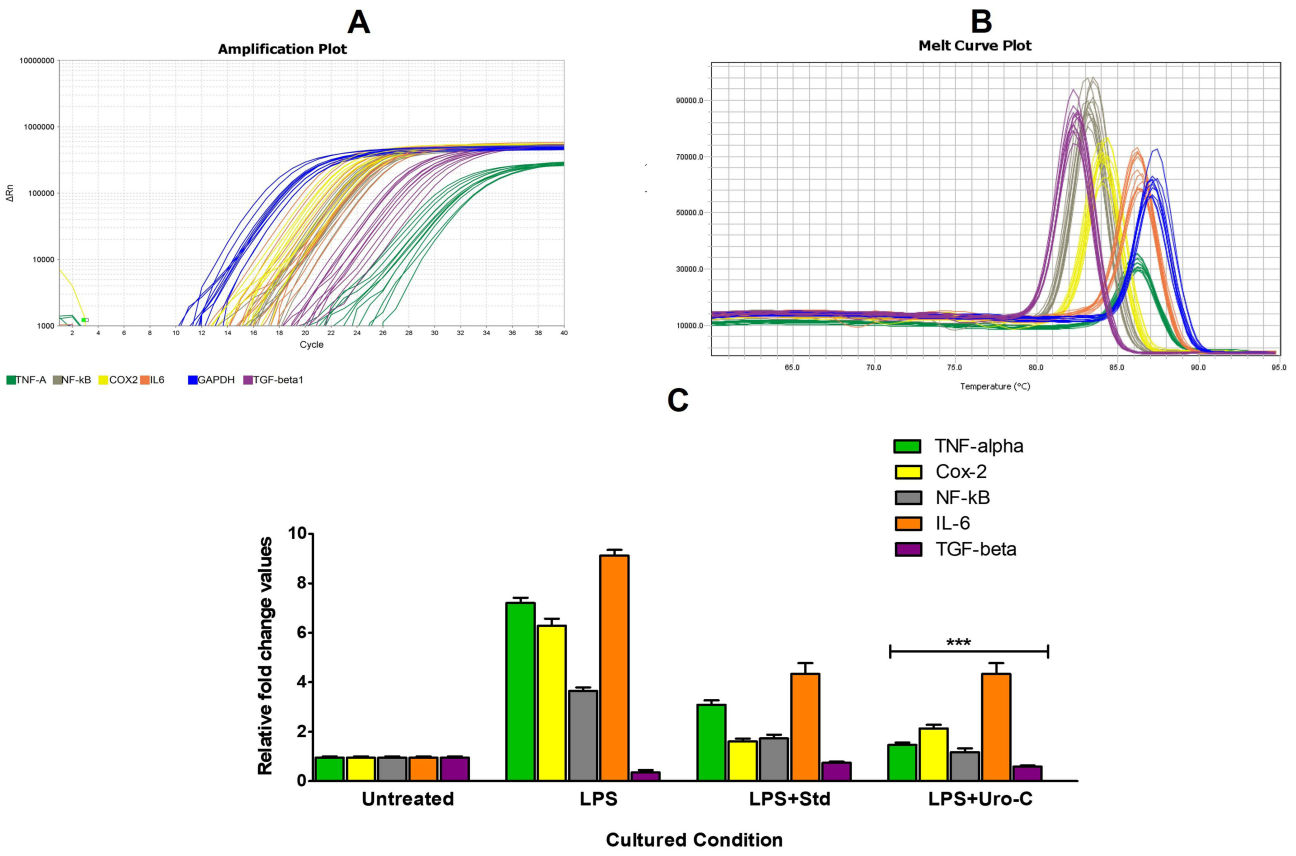

Figure 12 Effect of Urolithin-C on pro/anti-inflammatory cytokines gene expression by RT-qPCR: (**A**) Amplification of isolated cDNA of given samples with respective target genes (TNF-alpha, NF-κB, Cox-2, IL6 and TGF-beta1) obtained by RT-qPCR. All the Genes were amplified well without any errors. (**B**) Melt curves of all target genes along with housekeeping gene GAPDH (Glyceraldehyde-3-Phosphate Dehydrogenase) of treated and non-treated conditions of LPS induced RAW 264.7 cells by RT-qPCR method. (**C**) The relative mRNA expression of target genes (TNF-alpha, Cox-2, NF-kB, IL-6 and TGF-beta 1) in Untreated, LPS alone, DFC 1 mM and Urolithin-C with 25 µg/mL and 1 µg/mL of LPS pre-treatment treated on RAW 264.7 cells after the incubation period of 24hrs by RT-qPCR method. The results are expressed as mean ± SEM (n = 2). Significance at $p \leq 0.05$, *** at $p \leq 0.001$.

inflammation. Interestingly, in LPS-stimulated RAW 264.7 macrophages, Urolithin-C controls the production of inducible enzyme Cycloxygenase-2 (Cox-2), pro-inflammatory cytokines like Interleukin-2 (IL-2), Interleukin-6 (IL-6) and Tumour necrosis factor-alpha (TNF-alpha) as well as enhances anti-inflammatory Tumour growth factor-beta 1 (TGF-beta1). Additionally, the well-known and crucial transcription factor NF-κB triggers the release of pro- and anti-inflammatory cytokines by LPS-stimulated RAW 264.7 macrophages. In the pathophysiology of inflammatory illnesses, it is supposed to show a key part.[60,61] Furthermore, the cytoplasm contains the NF-κB p50 and p65 subunits, which bind to the IκB protein in dormant cells. Upon cell activation by LPS or other pro-inflammatory stimuli, IκB kinase rapidly phosphorylates and degrades IκB from the IκB/NF-κB complex. Thus, NF-κB penetrates the nucleus and initiates the transcription of inflammation-related genes.[62,63] Therefore, blocking the NF-κB p65 signaling pathway is thought to be a key target and an effective treatment strategy for inflammatory diseases. Meanwhile, Cox-2 is a pro-inflammatory protein that is necessary for the synthesis of NO and PGE2.[64,65] Cox-2, TNF-alpha, NF-κB p65, and IL-6 gene expression was evaluated by RT-PCR analysis based on the previously provided data. Urolithin-C limited the formation of pro-inflammatory cytokines by significantly reducing LPS-induced phosphorylation of NF-κB p65. In LPS-induced RAW 264.7 cell lines, Urolithin-C effectively increased anti-inflammatory genes (TGF-beta1) while decreasing pro-inflammatory genes (Cox-2, TNF-alpha, NF-kB, and IL-6). By blocking MAPK pathway, triterpenoids and their derivatives have shown anti-inflammatory properties. Ursolic acid (UA), for instance, inhibited the mitogen-induced phosphorylation of c-Jun NH2-terminal Kinase (JNK) and Extracellular Signal-Regulated Kinase (ERK) and deactivated the immunomodulatory transcription factors AP-1, NF-AT, and NF-κB in T and B cells.[66] In LPS-stimulated

https://doi.org/10.2147/JIR.S539273

macrophages, lupeol was reported to inhibit the production of pro-inflammatory cytokines TNF-α and IL-β.[67] Quercitrin, sinapic acid, and elemolic acid shown anti-inflammatory properties by blocking secretory phospholipase A2.[1,2,68]

Conclusion

Urolithin-C, a naturally occurring gut metabolite was successfully synthesized using a chemical method and characterized with versatile techniques. By suppressing heat-induced hemolysis, protein denaturation, and trypsin activity, Urolithin-C exhibited anti-inflammatory property. Most significantly, LPS-induced RAW 264.7 macrophages produced higher amounts of pro-inflammatory inducible enzyme (Cox-2), cytokines (IL-2, IL6 and TNF-alpha) and lower amounts of anti-inflammatory (TGF-beta1). Urolithin-C limits the production of pro-inflammatory cytokines by significantly reducing LPS-induced phosphorylation of NF-κB p65. These findings support the therapeutic potential of synthetic Urolithin-C as a novel anti-inflammatory agent, warranting further in vivo and pharmacokinetic studies.

Abbreviations

Uro-C, Urolithin-C; DFC, diclofenac; BSA, bovine serum albumin; LPS, Lipopolysaccharide; IL-1β, interleukin-1β; IL-6, interleukin-6: TNF-α, tumor necrosis factor-α; Cox-2, Cycloxygenase-2; TGF-beta1, Tumor growth factor-beta 1; NF-κB, Nuclear Factor-kappa B; TNF-α, tumor necrosis factor-α; TLRs, toll-like receptors; MAPK, mitogen-activated protein kinase; JAK-STAT, Janus kinase-signal transducer and activator of transcription; NSAIDs, nonsteroidal anti-inflammatory drugs; GAPDH, glyceraldehyde-3-phosphate dehydrogenase; ET, ellagitannins; EA, ellagic acid; HPLC, High-Performance Liquid Chromatography; TLC, Thin Layer Chromatography; FTIR, Fourier Transform Infrared Spectroscopy; NMR, Nuclear Magnetic Resonance; LC-MS, Liquid Chromatography-Mass Spectroscopy; PBS, phosphate-buffered saline.

Institutional Review Board Statement

The human blood sample was collected from the healthy individuals who were non-smokers and non-alcoholic as well. Before drawing the blood from the donors, purpose of the study was explained and written informed consent was obtained from the blood donors. Most importantly, experiments were conducted in accordance with the declaration and were approved by the Institutional Review Board (Institutional Review Board of Human Ethical Committee Tumkur University, Tumkur) protocol code Tu: DEV-02:2019-20/4748. It is to state that none of the patients blood was used for the study.

Acknowledgments

The Poornayu Research Labs in Bangalore, Karnataka, are gratefully acknowledged by the author for lending their facility for the characterization of synthesized Urolithin-C. Dharmappa K.K. gratefully acknowledges the funding support by DST-SERB [EEQ/2019/000456] dated 19th December 2019.

Disclosure

The authors report no conflicts of interest in this work.

References

1. Sophiya P, Urs D, Lone J K, et al. Quercitrin neutralizes sPLA2IIa activity, reduces the inflammatory IL-6 level in PC3 cell lines, and exhibits anti-tumor activity in the EAC-bearing mice model. *Front Pharmacol*. 2022;13:996285. doi:10.3389/fphar.2022.996285
2. Giresha AS, Urs D, Pundalik S, et al. Sinapicacid inhibits group iia secretory phospholipase a2 and its inflammatory response in mice. *Antioxidants*. 2022;11(7):1251. doi:10.3390/antiox11071251
3. Müller L, Di Benedetto S, Müller V. From homeostasis to neuroinflammation: insights into cellular and molecular interactions and network dynamics. *Cells*. 2025;14(1):54. doi:10.3390/cells14010054
4. Johnkennedy N, Mercy OC. Perspective of inflammation and inflammation markers. *JLMH*. 2022;3(1):16–26. doi:10.37899/journallamedihealtico.v3i1.620
5. lun LJ, Hui LY, Liu C, et al. Indirubin inhibits LPS-induced inflammation via TLR4 abrogation mediated by the NF-kB and MAPK signaling pathways. *Inflammation*. 2017;40(1):1–12. doi:10.1007/s10753-016-0447-7

6. Hayashi C, Gudino CV, Gibson Iii FC, Genco CA. REVIEW: pathogen-induced inflammation at sites distant from oral infection: bacterial persistence and induction of cell-specific innate immune inflammatory pathways: pathogen-induced inflammation. *Mol Oral Microbiol*. 2010;25 (5):305–316. doi:10.1111/j.2041-1014.2010.00582.x
7. Linghu KG, Xiong SH, Zhao GD, et al. Sigesbeckia orientalis l. Extract alleviated the collagen type ii–induced arthritis through inhibiting multi-target–mediated synovial hyperplasia and inflammation. *Front Pharmacol*. 2020;11:547913. doi:10.3389/fphar.2020.547913
8. Ageeva T, Rizvanov A, Mukhamedshina Y. Nf-κb and jak/stat signaling pathways as crucial regulators of neuroinflammation and astrocyte modulation in spinal cord injury. *Cells*. 2024;13(7):581. doi:10.3390/cells13070581
9. Yang L, He J. Anti-inflammatory effects of flavonoids and phenylethanoid glycosides from Hosta plantaginea flowers in LPS-stimulated RAW 264.7 macrophages through inhibition of the NF-κB signaling pathway. *BMC Complement Med Ther*. 2022;22(1):55. doi:10.1186/s12906-022-03540-1
10. Hu TY, Ju JM, Mo LH, et al. Anti-inflammation action of xanthones from Swertia chirayita by regulating COX-2/NF-κB/MAPKs/Akt signaling pathways in RAW 264.7 macrophage cells. *Phytomedicine*. 2019;55:214–221. doi:10.1016/j.phymed.2018.08.001
11. Jeong DE, Shim SY, Lee M. Anti-inflammatory activity of phenylpropyl triterpenoids from Osmanthus fragrans var. aurantiacus leaves. *Int Immunopharmacol*. 2020;86:106576. doi:10.1016/j.intimp.2020.106576
12. Fang Y, Wang H, Xia X, Yang L, He J. Kaempferol 3-O-(2G-glucosylrutinoside)-7-O-glucoside isolated from the flowers of Hosta plantaginea exerts anti-inflammatory activity via suppression of NF-κB, MAPKs and Akt pathways in RAW 264.7 cells. *Biomed Pharmacother*. 2022;153:113295. doi:10.1016/j.biopha.2022.113295
13. Yang L, Liu R, Ouyang S, et al. Compounds drg and dag, two phenol glycosides, inhibit tnf-α-stimulated inflammatory response through blocking nf-kb/akt/jnk signaling pathways in mh7a cells. *Inflammation*. 2021;44(5):1762–1770. doi:10.1007/s10753-021-01452-9
14. Liu Y, Chen W, Zheng F, Yu H, Wei K. Xanthatin alleviates LPS-induced inflammatory response in RAW264. 7 macrophages by inhibiting NF-κB, MAPK and stats activation. *Molecules*. 2022;27(14):4603. doi:10.3390/molecules27144603
15. Merecz-Sadowska A, Sitarek P, Śliwiński T, Zajdel R. Anti-inflammatory activity of extracts and pure compounds derived from plants via modulation of signaling pathways, especially pi3k/akt in macrophages. *IJMS*. 2020;21(24):9605. doi:10.3390/ijms21249605
16. Karin M, Ben-Neriah Y. Phosphorylation meets ubiquitination: the control of nf-κb activity. *Annu Rev Immunol*. 2000;18(1):621–663. doi:10.1146/annurev.immunol.18.1.621
17. Zheng Y, Liu S, Fan C, et al. Holistic quality evaluation of Qingwen Baidu Decoction and its anti-inflammatory effects. *J Ethnopharmacol*. 2020;263:113145. doi:10.1016/j.jep.2020.113145
18. Linghu KG, Zhao GD, Xiong W, et al. Comprehensive comparison on the anti-inflammatory effects of three species of Sigesbeckia plants based on NF-κB and MAPKs signal pathways in vitro. *J Ethnopharmacol*. 2020;250:112530. doi:10.1016/j.jep.2019.112530
19. Nk A, Kant S. Targeting inflammation in diabetes: newer therapeutic options. *World J Diab*. 2014;5(5):697–710. doi:10.4239/wjd.5.i5.697
20. Pollack RM, Donath MY, LeRoith D, Leibowitz G. Anti-inflammatory agents in the treatment of diabetes and its vascular complications. *Diabetes Care*. 2016;39(Supplement_2):S244–S252. doi:10.2337/dcS15-3015
21. Charlton A, Garzarella J, Jandeleit-Dahm KAM, Jha JC. Oxidative stress and inflammation in renal and cardiovascular complications of diabetes. *Biology*. 2020;10(1):18. doi:10.3390/biology10010018
22. Steven S, Frenis K, Oelze M, et al. Vascular inflammation and oxidative stress: major triggers for cardiovascular disease. *Oxid Med Cell Longev*. 2019;2019:1–26. doi:10.1155/2019/7092151
23. Fürst R, Zündorf I. Plant-derived anti-inflammatory compounds: hopes and disappointments regarding the translation of preclinical knowledge into clinical progress. *Mediators Inflamm*. 2014;2014:1–9. doi:10.1155/2014/146832
24. Espín JC, Larrosa M, García-Conesa MT, Tomás-Barberán F. Biological significance of urolithins, the gut microbial ellagic acid-derived metabolites: the evidence so far. *Evid Based Complement Alternat Med*. 2013;2013:1–15. doi:10.1155/2013/270418
25. Gil MI, Tomás-Barberán FA, Hess-Pierce B, Holcroft DM, Kader AA. Antioxidant activity of pomegranate juice and its relationship with phenolic composition and processing. *J Agric Food Chem*. 2000;48(10):4581–4589. doi:10.1021/jf000404a
26. Tomás-Barberán FA, González-Sarrías A, García-Villalba R, et al. Urolithins, the rescue of "old" metabolites to understand a "new" concept: metabotypes as a nexus among phenolic metabolism, microbiota dysbiosis, and host health status. *Mol Nutr Food Res*. 2017;61(1):1500901. doi:10.1002/mnfr.201500901
27. Mertens-Talcott SU, Jilma-Stohlawetz P, Rios J, Hingorani L, Derendorf H. Absorption, metabolism, and antioxidant effects of pomegranate (*punica granatum* l.) polyphenols after ingestion of a standardized extract in healthy human volunteers. *J Agric Food Chem*. 2006;54 (23):8956–8961. doi:10.1021/jf061674h
28. Seeram NP, Aronson WJ, Zhang Y, et al. Pomegranate ellagitannin-derived metabolites inhibit prostate cancer growth and localize to the mouse prostate gland. *J Agric Food Chem*. 2007;55(19):7732–7737. doi:10.1021/jf071303g
29. Karim S, Madani B, Burzangi AS, et al. Urolithin a's antioxidative, anti-inflammatory, and antiapoptotic activities mitigate doxorubicin-induced liver injury in wistar rats. *Biomedicines*. 2023;11(4):1125. doi:10.3390/biomedicines11041125
30. Bobowska A, Granica S, Filipek A, et al. Comparative studies of urolithins and their Phase II metabolites on macrophage and neutrophil functions. *Eur J Nutr*. 2021;60(4):1957–1972. doi:10.1007/s00394-020-02386-y
31. Lee G, Park J-S, Lee E-J, Ahn J-H, Kim H-S. Anti-inflammatory and antioxidant mechanisms of urolithin B in activated microglia. *Phytomedicine*. 2019:50–57. doi:10.1016/j.phymed.2018.06.032
32. Nealmongkol P, Tangdenpaisal K, Sitthimonchai S, Ruchirawat S, Thasana N. Cu(I)-mediated lactone formation in subcritical water: a benign synthesis of benzopyranones and urolithins A–C. *Tetrahedron*. 2013;69(44):9277–9283. doi:10.1016/j.tet.2013.08.045
33. Lin IC, Wu JY, Fang CY, Wang SC, Liu YW, Ho ST. Absorption and metabolism of urolithin a and ellagic acid in mice and their cytotoxicity in human colorectal cancer cells. *Evid Based Complement Alternat Med*. 2023;2023(1):8264716. doi:10.1155/2023/8264716
34. Battisti UM, Monjas L, Akladios F, et al. Exploration of novel urolithin c derivatives as non-competitive inhibitors of liver pyruvate kinase. *Pharmaceuticals*. 2023;16(5):668. doi:10.3390/ph16050668
35. Yin P, Zhang J, Yan L, et al. Urolithin C, a gut metabolite of ellagic acid, induces apoptosis in PC12 cells through a mitochondria-mediated pathway. *RSC Adv*. 2017;7(28):17254–17263. doi:10.1039/C7RA01548H
36. Wongsa P, Phatikulrungsun P, Prathumthong S. FT-IR characteristics, phenolic profiles and inhibitory potential against digestive enzymes of 25 herbal infusions. *Sci Rep*. 2022;12(1):6631. doi:10.1038/s41598-022-10669-z

37. Tang L, Jiang J, Song G, et al. Design, synthesis, and biological evaluation of novel urolithins derivatives as potential phosphodiesterase II inhibitors. *Sci Rep*. 2021;11(1):23792. doi:10.1038/s41598-021-03194-y
38. Denis C, Methia N, Frenette PS, et al. A mouse model of severe von Willebrand disease: defects in hemostasis and thrombosis. *Proc Natl Acad Sci USA*. 1998;95(16):9524–9529. doi:10.1073/pnas.95.16.9524
39. D'Arcy PF, Howard EM. A new anti-inflammatory test, utilizing the chorio-allantoic membrane of the chick embryo. *Brit J Pharmacol Chemother*. 1967;29(3):378–387. doi:10.1111/j.1476-5381.1967.tb01969.x
40. Mizushima Y, Kobayashi M. Interaction of anti-inflammatory drugs with serum proteins, especially with some biologically active proteins. *J Pharm Pharmacol*. 1968;20(3):169–173. doi:10.1111/j.2042-7158.1968.tb09718.x
41. Revankar AG, Bagewadi ZK, Shaikh IA, et al. In-vitro and computational analysis of Urolithin-A for anti-inflammatory activity on Cyclooxygenase 2 (COX-2). *Saudi J Biol Sci*. 2023;30(11):103804. doi:10.1016/j.sjbs.2023.103804
42. Lee S, Choi H, Park Y, et al. Urolithin and reduced urolithin derivatives as potent inhibitors of tyrosinase and melanogenesis: importance of the 4-substituted resorcinol moiety. *IJMS*. 2021;22(11):5616. doi:10.3390/ijms22115616
43. Van Meerloo J, Kaspers GJL, Cloos J. Cell sensitivity assays: the mtt assay. *Cancer Cell Culture*. 2011;731:237–245. doi:10.1007/978-1-61779-080-5_20
44. Livak KJ, Schmittgen TD. Analysis of relative gene expression data using real-time quantitative pcr and the 2−δδct method. *Methods*. 2001;25(4):402–408. doi:10.1006/meth.2001.1262
45. Jannus F, Medina-O'Donnell M, Neubrand VE, et al. Efficient in vitro and in vivo anti-inflammatory activity of a diamine-pegylated oleanolic acid derivative. *IJMS*. 2021;22(15):8158. doi:10.3390/ijms22158158
46. Yu H, Gao R, Liu Y, Fu L, Zhou J, Li L. Stimulus-responsive hydrogels as drug delivery systems for inflammation targeted therapy. *Adv Sci*. 2024;11(1):2306152. doi:10.1002/advs.202306152
47. Chaachouay N, Zidane L. Plant-derived natural products: a source for drug discovery and development. *DDC*. 2024;3(1):184–207. doi:10.3390/ddc3010011
48. Venkatappa MM, Udagani C, Hanume Gowda SM, et al. Green synthesised tio2 nanoparticles-mediated terenna asiatica: evaluation of their role in reducing oxidative stress, inflammation and human breast cancer proliferation. *Molecules*. 2023;28(13):5126. doi:10.3390/molecules28135126
49. Venkataramaiah S, Venkatappa MM, Udagani C, Sannaningaiah D. Green-synthesized cobalt ferrite nanoparticle alleviated sodium nitrite-induced oxidative stress through its anti-oxidant property and displayed anti-inflammatory, anti-diabetic and anti-platelet activities. *J Supercond Nov Magn*. 2024;37(11–12):1839–1857. doi:10.1007/s10948-024-06813-7
50. Hanumegowda SM, Srinivasa C, Shivaiah A, et al. Kenaf seed cysteine protease (Kscp) inhibits the intrinsic pathway of the blood coagulation cascade and platelet aggregation. *CPPS*. 2024;25(5):394–408. doi:10.2174/0113892037265109231114065204
51. Gutiérrez-Pacheco MM, Torres-Moreno H, Flores-Lopez ML, et al. Mechanisms and applications of citral's antimicrobial properties in food preservation and pharmaceuticals formulations. *Antibiotics*. 2023;12(11):1608. doi:10.3390/antibiotics12111608
52. Venkatappa MM, Udagani C, Hanumegowda SM, et al. Effect of biofunctional green synthesized mgo-nanoparticles on oxidative-stress-induced tissue damage and thrombosis. *Molecules*. 2022;27(16):5162. doi:10.3390/molecules27165162
53. Imaga NA, Chukwu CE, Blankson A, Gbenle GO. Biochemical assessment of Ciklavit®, a nutraceutical used in sickle cell anaemia management. *J Herbal Med*. 2013;3(4):137–148. doi:10.1016/j.hermed.2013.05.003
54. Othman A, Sekheri M, Filep JG. Roles of neutrophil granule proteins in orchestrating inflammation and immunity. *FEBS J*. 2022;289(14):3932–3953. doi:10.1111/febs.15803
55. Assiry AA, Bhavikatti SK, Althobaiti FA, Mohamed RN, Karobari MI. Evaluation of *in vitro* antiprotease activity of selected traditional medicinal herbs in dentistry and its in silico pass prediction. *Biomed Res Int*. 2022;2022(1):5870443. doi:10.1155/2022/5870443
56. Laskin DL. Macrophages and inflammatory mediators in chemical toxicity: a battle of forces. *Chem Res Toxicol*. 2009;22(8):1376–1385. doi:10.1021/tx900086v
57. Kang SR, Han DY, Park KI, et al. Suppressive effect on lipopolysaccharide-induced proinflammatory mediators by *citrus aurantium l*. in macrophage RAW 264. 7 cells via nf- κ b signal pathway. *Evid Based Complement Alternat Med*. 2011;2011(1):248592. doi:10.1155/2011/248592
58. McWhorter FY, Wang T, Nguyen P, Chung T, Liu WF. Modulation of macrophage phenotype by cell shape. *Proc Natl Acad Sci USA*. 2013;110(43):17253–17258. doi:10.1073/pnas.1308887110
59. Zhang H, Dhalla NS. The role of pro-inflammatory cytokines in the pathogenesis of cardiovascular disease. *IJMS*. 2024;25(2):1082. doi:10.3390/ijms25021082
60. Tian Y, Zhou S, Takeda R, Okazaki K, Sekita M, Sakamoto K. Anti-inflammatory activities of amber extract in lipopolysaccharide-induced RAW 264.7 macrophages. *Biomed Pharmacother*. 2021;141:111854. doi:10.1016/j.biopha.2021.111854
61. Correa LB, Seito LN, Manchope MF, et al. Methyl gallate attenuates inflammation induced by Toll-like receptor ligands by inhibiting MAPK and NF-Kb signaling pathways. *Inflamm Res*. 2020;69(12):1257–1270. doi:10.1007/s00011-020-01407-0
62. Wang L, Gu J, Zong M, et al. Anti-inflammatory action of physalin A by blocking the activation of NF-κB signaling pathway. *J Ethnopharmacol*. 2021;267:113490. doi:10.1016/j.jep.2020.113490
63. Han JM, Lee EK, Gong SY, Sohng JK, Kang YJ, Jung HJ. Sparassis crispa exerts anti-inflammatory activity via suppression of TLR-mediated NF-κB and MAPK signaling pathways in LPS-induced RAW264.7 macrophage cells. *J Ethnopharmacol*. 2019;231:10–18. doi:10.1016/j.jep.2018.11.003
64. Liao W, He X, Yi Z, Xiang W, Ding Y. Chelidonine suppresses LPS-Induced production of inflammatory mediators through the inhibitory of the TLR4/NF-κB signaling pathway in RAW264.7 macrophages. *Biomed Pharmacother*. 2018;107:1151–1159. doi:10.1016/j.biopha.2018.08.094
65. Zou YH, Zhao L, Xu YK, et al. Anti-inflammatory sesquiterpenoids from the Traditional Chinese Medicine Salvia plebeia: regulates pro-inflammatory mediators through inhibition of NF-κB and Erk1/2 signaling pathways in LPS-induced RAW264.7 cells. *J Ethnopharmacol*. 2018;210:95–106. doi:10.1016/j.jep.2017.08.034
66. Checker R, Sandur SK, Sharma D, et al. Potent anti-inflammatory activity of ursolic acid, a triterpenoid antioxidant, is mediated through suppression of nf-κb, ap-1 and nf-at. *PLoS One*. 2012;7(2):e31318. doi:10.1371/journal.pone.0031318
67. Fernández MA, De Las Heras B, Garcia MD, Sáenz MT, Villar A. New insights into the mechanism of action of the anti-inflammatory triterpene lupeol. *J Pharm Pharmacol*. 2001;53(11):1533–1539. doi:10.1211/0022357011777909
68. Giresha AS, Urs D, Manjunatha JG, et al. Group IIA secreted phospholipase A2 inhibition by elemolic acid as a function of anti-inflammatory activity. *Sci Rep*. 2022;12(1):7649. doi:10.1038/s41598-022-10950-1